Source Rock Evaluation and Petroleum System Modeling of the East Beni Suef Basin, North Eastern Desert, Egypt

Ahmed Y. Tawfik[a,b*], R. Ondrak[c], G. Winterleitner[a], M. Mutti[a]

[a] Institute of Geosciences, University of Potsdam, Campus Golm / Building 27 Karl Liebknecht-Str. 24-25 14476 Potsdam, Germany

[b] Geology Department, Faculty of Science, Suez University, Suez, Egypt

[c] Section Organic Geochemistry, Helmholtz Centre Potsdam GFZ German Research Centre for Geosciences, Telegrafenberg, 14473 Potsdam, Germany

[*] Corresponding author: yousef1@uni-potsdam.de (A. Y. Tawfik)

Highlights

- Three kerogen types (II, II/III, and III) are defined in the East Beni Suef Basin.
- Abu Roash "F" Member is the main source rock and exists in the early oil window.
- Four tectonic episodes can be inferred from the reconstructed burial history.
- Sedimentation onset and rates differ across both sides of the Beni Suef Basin.
- Erosion and heat flow have proportional and mutual effects on thermal maturity.

Abstract

This study deals with the East Beni Suef Basin (Eastern Desert, Egypt) and aims to evaluate the source-generative potential, reconstruct the burial and thermal history, examine the most influential parameters on thermal maturity modeling, and improve on the models already published for the West Beni Suef to ultimately formulate a complete picture of the whole basin evolution. Source rock evaluation was carried out based on TOC, Rock-Eval pyrolysis, and visual kerogen petrography analyses. Three kerogen types (II, II/III, and III) are distinguished in the East Beni Suef Basin, where the Abu Roash "F" Member acts as the main source rock with good to excellent source potential, oil-prone mainly type II kerogen, and immature to marginal maturity levels. The burial history shows four depositional and erosional phases linked with the tectonic evolution of the basin. A hiatus (due to erosion or non-deposition) has occurred during the Late Eocene-Oligocene in the East Beni Suef Basin, while the West Beni Suef Basin has continued subsiding. Sedimentation began later (Middle to Late Albian) with lower rates in the East Beni Suef Basin compared with the West Beni Suef Basin (Early Albian). The Abu Roash "F" source rock exists in the early oil window with a present-day transformation ratio of about 19 % and 21 % in the East and West Beni Suef Basin, respectively, while the Lower Kharita source rock, which is only recorded in the West Beni Suef Basin, has reached the late oil window with a present-day transformation ratio of about 70 %. The magnitude of erosion and heat flow have proportional and mutual effects on thermal maturity. We present three possible scenarios of basin modeling in the East Beni Suef Basin concerning the erosion from the Apollonia and Dabaa formations. Results of this work can serve as a basis for subsequent 2D and/or 3D basin modeling, which are highly recommended to further investigate the petroleum system evolution of the Beni Suef Basin.

Keywords

Source Rock Evaluation; Kerogen Petrography; Basin Modeling; Sensitivity Analysis; Beni Suef Basin; Egypt.

1. Introduction

The Beni Suef Basin is an extensional rift basin in north-central Egypt lying approximately 150 km south of Cairo and is bisected by the Nile Valley into the West and East of the Nile Provinces (Fig. 1). Recently, the Beni Suef Basin is fast emerging as one of the most promising and prolific targets for hydrocarbon exploration with success providing an ample incentive for exploring the petroleum systems of Upper Egypt (Zahran et al., 2011). The promising exploration of the Beni Suef oil field in September 1997 by Seagull Energy Corporation emphasized a new productive basin extends eastward across the Nile River (Nemec and Colley, 1998), which triggered Qarun Petroleum Company to continue the exploration activities on the eastern side of the Beni Suef Basin, which resulted in the discovery of Gharibon and Sohba oil fields in 2002 and 2008, respectively (Zahran et al., 2011).

Although the East Beni Suef Basin constitutes the major portion of Beni Suef Basin (Zahran et al., 2011), most of the published work focused on the West Beni Suef Basin (Makky et al., 2014; Khalil et al., 2016; Abd El-Gawad et al., 2017; Abdel-Fattah et al., 2017; El-Werr et al., 2017; Elanbaawy et al., 2017; Shehata et al., 2018a, 2018b, 2019; Sakran et al., 2019; Edress et al., 2021), while little has been published on the East Beni Suef Basin (Abd El-Aal et al., 2015; Saber and Salama, 2017; Salem and Sehim, 2017; Tahoun et al., 2017; Rabeh et al., 2019) with no detailed focus on the hydrocarbon source potential and basin modeling.

The present work deals with the East Beni Suef Basin and endeavors to assess the hydrocarbon-generative potential of the Upper Cretaceous-Middle Eocene sedimentary sequence, reconstruct the burial and thermal history, determine the timing of hydrocarbon generation, and improve the published models on the West Beni Suef Basin to formulate a complete picture of the source rock characterization and basin evolution through the whole basin. Furthermore, the most influential parameters on thermal maturity modeling are examined through sensitivity analysis to minimize the inherent uncertainty of basin modeling, where the impacts of the Syrian-Arc system tectonics and the Miocene thermal uplift of the Red Sea rifting on the source rock maturity are discussed for a more realistic and robust basin modeling.

To achieve these goals, we used an extensive data set of geochemical and kerogen analyses including total organic carbon (TOC), Rock-Eval pyrolysis, and visual kerogen composition that were performed on 190 cutting samples from three wells in the East Beni Suef Basin (i.e., Gharibon-1X, Gharibon NE-1x, and Tareef-1x). PetroMod 1D basin modeling software (Schlumberger; Version 2019) was used to construct the burial and thermal history and to perform the sensitivity analysis.

2. Geological Setting

The sedimentary basins of NE Africa were initiated under tensional tectonics in the wake of the post-Hercynian break-up of Gondwana (Guiraud, 1998; Keeley and Massoud, 1998; Macgregor and Moody, 1998; Badalini et al., 2002; Tawadros, 2011; Wood, 2015) probably attributed to mantle-upwelling during Gondwana disintegration (Storey, 1995, 1996; Wilson et al., 1998; Hawkesworth et al., 1999), leading to the development of extensional half-grabens that formed along the southern margin of the Neo-Tethys Ocean (Wood, 2015; Abdel-Fattah et al., 2020, 2021). The Beni Suef Basin experienced an initial Albian extensional phase in the NE-SW direction and a transtentional phase during the Santonian time (Zahran et al., 2011; Abd El-Aal et al., 2015; Salem and Sehim, 2017), these tectonics could be attributed to the relative motion of Africa with respect to Eurasia (Smith, 1971; Meshref, 1990; Moustafa, 2008). The extensional rifting resumed within the basin during the Eocene time (Salem and Sehim, 2017), while a significant uplift took place during the Miocene in response to the pre-rift thermal uplift of the Red Sea (Bosworth and Stockli, 2016; Abdelbaset et al., 2020).

The sedimentary section of both sides of the Beni Suef Basin is well correlated (Zahran et al., 2011; Salem and Sehim, 2017; Shehata et al., 2018b, 2020), except for the absence of the Albian Lower Kharita shales -the most thermal mature source rock in the West Beni Suef Basin- and the Oligocene Dabaa Formation in the East Beni Suef Basin (Fig. 2).

The stratigraphic column of the East Beni Suef Basin starts with the continental clastics of the Albian Kharita Formation, which is overlain by the shallow marine clastics of the Early Cenomanian Bahariya Formation (Fig. 2). The Late Cenomanian reflects a widespread marine transgression, which resulted in the deposition of the first carbonate succession Abu Roash Formation with sandstone, siltstone, and shale interbeds (Hantar, 1990; Dolson et al., 2014). Based on the clastic to carbonate ratio, the Late Cenomanian-Santonian Abu Roash Formation is divided into seven members from base to top: "G" through "A" (Fig. 2). Members "B", "D", and "F" are relatively clean carbonates, whereas the other members contain considerable amounts of clastic sediments (Said, 1962; Norton, 1967; EGPC, 1992). The Abu Roash Formation was dominated by neritic to open marine conditions (El Beialy et al., 2010, 2011; El-Soughier et al., 2014; Shehata et al., 2019), with an exception for the "G" Member, which was deposited under Lagoonal conditions (Hantar, 1990; Shehata et al., 2021). The Chalk of the Campanian-Maastrichtian Khoman Formation represents the top of the Cretaceous sequence and unconformably underlies the Lower-Middle Eocene Apollonia Formation that crops out in the study area.

3. Materials and Methods

A total of 190 cutting samples were collected from three wells (i.e., 40 samples from Gharibon-1X, 68 samples from Gharibon NE-1X, and 82 samples from Tareef-1X) in the East Beni Suef Basin (Fig. 1). Geochemical analyses (total organic carbon (TOC) and Rock-Eval pyrolysis) and organic petrology (Thermal Alteration Index (TAI), petrographic kerogen typing, and vitrinite reflectance (%R_o) were performed by the StratoChem Services Company, New Maadi, Cairo, Egypt and made accessible through the Egyptian General Petroleum Corporation in collaboration with the Qarun Petroleum Company.

Measured pyrolysis parameters include the quantity of preexisting volatile hydrocarbons within the sample (S1), hydrocarbons that evolved from the thermal cracking of kerogen (S2), the amount of carbon dioxide derived from kerogen pyrolysis (S3), and the maximum pyrolysis temperature at which the S2 peak occurs (T_{max}). Hydrogen Index (HI), Oxygen Index (OI), and Production Index (PI) were derived according to Peters (1986) and Peters et al. (2005).

1D basin and petroleum system modeling was performed using PetroMod software (Schlumberger; Version 2019) at the Institute of Geosciences, Potsdam University. Tareef-1X well was chosen as a representative location to reconstruct the burial and thermal history and estimate the timing of hydrocarbon generation because it has the most complete dataset of vitrinite reflectance and temperature for calibration. The input data for the basin modeling including the stratigraphic units, depositional ages, lithologies, depths to the tops of the rock units, and sedimentation events (e.g., deposition, erosion, and hiatus) were defined from well reports and previous studies. Boundary conditions including paleo water depth (PWD), sediment water interface temperature (SWIT), and basal heat flow (HF) were set according to the general tectonostratigraphic evolution of the basin to define the basic energetic conditions within the basin. Easy %R_o model of Sweeney and Burnham, (1990) was used to calculate the vitrinite reflectance, which was calibrated using measured vitrinite reflectance (%R_o). A sensitivity analysis was conducted to examine the most influential parameters of input data and boundary conditions in basin modeling.

4. Results and Discussion

4.1. Source Rock Evaluation

Measurements of the geochemical analyses including TOC and Rock-Eval pyrolysis are listed in Tables 1-3. A cutoff point of 0.5 wt% TOC was selected to exclude the organic-lean samples from further analyses because of the minimal hydrocarbon-source potential of those samples. The geochemical analyses were interpreted according to the guidelines of Peters et al. (2005).

4.1.1. Organic Matter Richness and Quality

The Apollonia Formation ranges in TOC between 0.53 to 2.77 wt% and S2 from 2.36 to 18.30 mg HC/g rock (Table 1) indicating fair to very good source potential (Fig. 3) with oil-prone predominantly type II kerogen as suggested from its high HI (358 to 692 mg HC/g TOC) (Fig.4 and Table 1). The sample at 365.76 m in Gharibon-1X well has an anomalous high HI (889 mg HC/g TOC) compared with the uniform trend of all samples, thus we considered it a nonrepresentative sample.

The Abu Roash “A” Member varies in TOC from 0.57 to 2.02 wt% and S2 from 1.23 to 9.68 mg HC/g (Table 2) rock denoting fair to good source potential (Fig. 3) with HI ranging from 134 to 657 mg HC/g TOC suggesting mixed oil- and gas-prone type II/III kerogen (Fig. 4). The Abu Roash “E” Member shows fair to very good source potential (Fig. 3) as indicated by its TOC (0.54-4.99 wt%) and S2 (0.31-12.52 mg HC/g rock) values (Table 2) with mainly gas-prone type III kerogen as indicated by its lower HI values (58-254 mg HC/g TOC) (Fig. 4 and Table 2).

The Abu Roash “F” Member ranges in TOC from 1.04 to 4.02 wt% and S2 from 3.55 to 27.91 mg HC/g rock (Table 2) indicating good to excellent source potential (Fig. 3) with high HI values between 341 to 713 mg HC/g TOC (Table 2) suggesting oil-prone mainly type II kerogen (Fig. 4). Only one sample from Tareef-1X shows the lowest HI (262 mg HC/g TOC), this could be attributed to organic matter degradation and/or to mineral matrix effect that can result in decreasing hydrogen index for samples with TOC less than 2% due to hydrocarbon retention on the mineral grains as indicated by the presence of shale streaks at this depth in the composite well reports.

The TOC and S2 values of Abu Roash “G” range from 0.51 to 2.76 wt% and 0.29 to 12.82 mg HC/g rock (Table 2), respectively denoting fair to very good source potential (Fig. 3) with mixed oil and gas-prone type II/III kerogen (Fig. 4) as suggested from its HI values (56-493 mg HC/g TOC) (Table 2). The Bahariya Formation reaches TOC content of 0.5 to 2.25 wt% and S2 of 0.54 to 4.43 mg HC/g rock (Table 3) indicating fair to good source potential (Fig. 3) with low HI values (109-286 mg HC/g TOC) (Table 3) suggesting mainly gas-prone type III kerogen (Fig. 4). Based on the general trend of the pyrolysis results within the Bahariya Formation, the sample at 2241.80 m in Tareef-1X well is anomalously showing very low values of S2 (0.13 mg HC/g rock) and HI (24 mg HC/g TOC) and the highest PI (0.41), so we regarded it as a nonindigenous sample, where T_{max} is spurious for S2 <0.2, hence we excluded it from further consideration (Peters, 1986).

TOC versus S2 plot (Fig. 3) indicates that TOC content is in line with S2 values and demonstrates a wide range of fair to excellent source potential. The Abu Roash "F" Member shows the highest hydrocarbon-generating potential and acts as the main source rock in the study area, while the Bahariya Formation and the Abu Roash "E" Member exhibit the lowest source potential. The very high HI values (>660 mg HC/g TOC) of some samples in the Apollonia and Abu Roash "F" Member showing a shift toward type I kerogen in Figure 4 is possibly due to variations of biological source as algal debris were incorporated into the sediments, or variation in the preservation conditions to be highly reducing. Thus, it should be emphasized that Rock-Eval pyrolysis is not sufficient in precisely defining the present kerogen types and needs to be strengthened by other evaluation techniques such as gas chromatography (Dembicki, 2009, 2017).

4.1.2. Organic Matter Maturity

Although vitrinite reflectance serves as a principal diagnostic technique for thermal maturity assessment, it is highly recommended to weigh it with other maturity tools to avoid misleading measurements (Peters and Cassa, 1994; McCarthy et al., 2011), thus we employed data from various maturity parameters (e.g. Vitrinite Reflectance (%R_o), pyrolysis temperature (T_{max}), Production Index (PI), and Thermal Alteration Index (TAI)) to obtain a coherent picture of maturity in the analyzed succession.

The vitrinite reflectance profiles show that most of the analyzed samples are immature to marginally mature (Fig. 5. a). The analyzed samples vary in vitrinite reflectance from 0.39 to 0.47% for Apollonia Formation, 0.49 to 0.56% for Abu Roash "A" Member, 0.57 to 0.71% for Abu Roash "E" Member, 0.49 to 0.62% for the Abu Roash "G" Member, and 0.42 to 0.6% for the Bahariya Formation (Table 4 and Fig. 5. a). Only one value was recorded for the vitrinite reflectance in the Abu Roash "F" Member (0.46%), the scarcity of vitrinite reflectance within the Abu Roash "F" Member is attributed to the dominant rich oil-prone kerogen (mainly composed of lipids), where the depositional setting has not received significant terrestrial organic matter. The vitrinite reflectance values for Abu Roash "G" Member and Bahariya Formation decrease with depth suggesting suppressed maturity data or caved sediments as indicated by the available geochemical logs, thus should be excluded from the calibration of the thermal modeling results. The plot of TAI demonstrates that the studied samples are clustered around immature to marginally mature stages (2-2.7), which strongly correlates with %R_o (Fig. 5. b and Table 4).

The Apollonia Formation ranges in T_{max} from 419 to 430 °C and PI from 0.04 to 0.16 (Fig. 6 and Table 1), indicating an immature stage. The Abu Roash "A" Member ranges in T_{max} from 424 to 438 °C and PI between 0.03 to 0.14 (Fig. 6 and Table 2) denoting immature to marginally mature stages. The Abu Roash "E" Member has T_{max} ranges from 310 to 443 °C and PI range between 0.06 to 0.23 indicating immature to mature stages (Fig. 6 and Table 2). The Abu Roash "F" Member ranges in T_{max} from 424 to 437 °C and PI from 0.09 to 0.18 (Fig. 6 and Table 2) showing immature to marginally mature stages.

The T_{max} values range from 274 to 445 °C for the Abu Roash "G" Member with PI range between 0.06 to 0.34 (Fig. 6 and Table 2) indicating immature to mature stages. The Bahariya Formation ranges in T_{max} from 368 to 446 °C and PI from 0.11 to 0.24 (Fig. 6 and Table 3) suggesting immature to mature stages.

4.2. Kerogen Data Analysis

Visual kerogen analysis represents an integral part of source rock evaluation through appraising the chemical and physical characteristics of kerogen and supplementing the pyrolysis techniques (Waples, 1985). Microscopic kerogen examination reveals that the upper Cretaceous-Eocene succession varies in maceral composition from liptinite to vitrinite with minor traces of inertinite (Table 4).

The Apollonia Formation and the Abu Roash "A" and "F" members contain a significant amount of liptinites -mainly unstructured lipids- with little vitrinite (Fig. 7) indicating oil-prone kerogen, while vitrinite macerals represent the main kerogen constituents in the Abu Roash "E" Member and the Bahariya Formation (Fig. 7) confirming gas-prone kerogen. The Abu Roash "G" Member contains a mixture of the three main macerals (Fig. 7) indicating a mixed oil/gas-prone kerogen, this heterogeneity of kerogen in the Abu Roash "G" Member arises from a mixture of terrigenous and marine organic matter due to variation in depositional conditions. Kerogen petrography of the examined sedimentary succession (Fig. 7) confirms the Rock-Eval pyrolysis results in terms of the different kerogen quality shown in Figure 4. As the unstructured lipids could originate from various biological sources with different depositional environments, palynofacies and/or biomarker studies are essential to investigate the origin of these unstructured lipids and to gain detailed insights into their depositional conditions (e.g. Peters et al., 2005; El Nady, 2008; El Beialy et al., 2010; El Diasty and Moldowan, 2013; Tahoun et al., 2017; Ghassal et al., 2018; Mohamed et al., 2020).

Based on the source rock evaluation, the analyzed samples of the upper Cretaceous-Eocene succession of the East Beni Suef Basin show a wide range of fair to excellent source rock potential, immature to marginally maturity levels, and three kerogen types (II, mixed II/III, and III). The low source rock potential of some rock units could be attributed to a deficiency in the organic matter production, preservation, and/or oxidizing depositional conditions. The thermal maturity derived from vitrinite reflectance (%R_o) correlates well with the thermal alteration index (TAI) but differs slightly from the determined maturity by T_{max} and PI due to procedural differences, where the vitrinite reflectance and TAI are defined from optical kerogen analysis, whereas the T_{max} and PI are based on Rock-Eval pyrolysis. The maturity profiles show a gradual increase with depth, except for the Abu Roash "G" Member and the Bahariya Formation, which could be attributed to suppressed maturity data or caved sediments. The low maturity levels of the East Beni Suef strata are the result of the relatively shallower burial and younger sedimentary succession (Albian-Eocene) compared with the much thicker and older succession (Paleozoic-Cenozoic) of the northern Western Desert basins (EGPC, 1992; Moustafa, 2008).

In general, the analyzed samples of the sedimentary units are distributed along most of the kerogen evolutionary pathways (Fig. 4) due to variations in the organic matter content (i.e., liptinite, vitrinite, and inertinite), which reflect different depositional environments of the sedimentary succession from lagoonal to open marine setting. Although the kerogen data analysis confirms the results of the Rock-Eval pyrolysis regarding the variation in the organic matter, a distinctive differentiation of the kerogen types of the Apollonia Formation and Abu

Roash "F" Member is infeasible, as the unstructured lipids can contribute to both type I and II kerogens (Jones, 1984; Tissot and Welte, 1984; Merrill, 1991).

Former studies on the Cretaceous sequence of the West Beni Suef Basin show similar results of kerogen types and source rock potential to these presented here for the East Beni Suef Basin. Makky et al. (2014) and Abdel-Fattah et al. (2017) defined three kerogen types (I/II (II), II/III, and III) with fair to very good organic matter richness and thermal maturity ranging from immature to postmature. Edress et al. (2021) reported five kerogen types (I, II, II/III, III, and IV) with fair to very good source potential and mature to postmature stages. Abd El-Gawad et al. (2017) studied only the source rock potential of the Abu Roash "F" Member and defined type I/II kerogen with good to very good hydrocarbon generative potential and immature to marginally mature levels.

4.3. Basin Modeling

4.3.1. Input Data and Boundary Conditions

A conceptual model for the geological history of the study area was first developed using the stratigraphic units, absolute age assignment, lithologic description, and geological events (deposition, erosion, and hiatus) based on the composite log reports of the studied wells and literature studies (Zahran et al., 2011; Abd El-Aal et al., 2015; El Batal et al., 2016; Salem and Sehim, 2017; Shehata et al., 2018b; Abdelbaset et al., 2020) (Table 5). According to the available well reports, the drilled stratigraphic succession of the East Beni Suef Basin does not record the Late Eocene-Oligocene Dabaa Formation, compared with the West Beni Suef Basin, thus a hiatus is suggested during this period, but the probability of the deposition and later complete erosion of the Dabaa Formation could be a possible scenario, which will be discussed later in the sensitivity analysis section.

For a more realistic representation and simulation, we created custom lithologies for Abu Roash Formation using PetroMod Lithology Editor based on the clastic to carbonate ratio to overcome the heterogeneity and reduce the uncertainty inherited by assigning a single lithology for a mixed section. Abu Roash "G" Member was further divided into three units based on the available composite well reports to define the reservoir and seal rocks.

Estimation of the eroded overburden thickness represents a crucial step in basin modeling procedures and has profound implications on the evolution of the petroleum systems within sedimentary basins (Poelchau, 2001; Corcoran and Doré, 2005). As a first estimation, we applied Dow's method (1977) and the stratigraphic correlation approach discussed by Corcoran and Doré (2005) to define the scale of erosion at the two erosional unconformities of Khoman and Apollonia formations. The maximum preserved section of the Khoman Formation (about 340 m) exists in the EON well, thus we suggest about 200 m of erosion has occurred at the top of the Khoman Formation in Tareef-1X well. Dow's method (1977) indicates about 300 m of erosion from the Apollonia Formation by projecting the %R_o profile to 0.2% at the present day surface (Fig. 8). In this case, we dealt with the basin as a continuously subsiding basin, where the erosional unconformity at the Khoman Formation has no impact on the present-day maturity levels as indicated by the uniform and relatively low maturity %R_o values across this unconformity (Fig. 5. a). Based on the two methods, a hundred-meter scale of erosion was defined at the top of the Khoman and Apollonia formations, while the absolute values are finely tunning during the basin modeling simulation.

Log-derived temperatures provide valuable constraints on the present-day geothermal regime of the subsurface strata, however, they must always be adjusted for the cooling effects of the circulating drilling fluids prior to any application in basin modeling (Evans and Coleman, 1974; Deming, 1989; Peters and Nelson, 2012; Dembicki, 2017; Aabø and Hermanrud, 2019). Several BHT correction procedures have been developed; most of them are summarized by Hermanrud et al. (1990) and Goutorbe et al. (2007). Corrected BHT for Tareef-1X well using the statistical method of Waples and Ramly (2001) (for shallow depths <3500 m) and the model put forward by Aabø and Hermanrud (2019) are about 111℃ and 115℃, respectively, which are quite similar. The corrected geothermal gradient to be used in model calibration is about 32 ℃/Km.

We defined the kinetics of kerogen cracking to oil and gas based on the organofacies type and the depositional age of the source rock (Mesozoic and younger). Thus, Pepper and Corvi's (1995)_TII(B) kinetic was assigned for the Abu Roash "F" source rock that contains marine organofacies type B (Abdelbaset et al., 2020).

Boundary conditions determine the basis of the energetic conditions for the temperature development of all rock units and the organic matter maturity history and strongly constrain the simulation quality. Boundary conditions to be assigned in basin modeling include paleo water depth (PWD), sediment water interface temperature (SWIT), and basal heat flow (HF) (Hantschel and Kauerauf, 2009) (Fig. 9).

The basal heat flow was initially defined in the context of the tectonic history of the basin following the concept of McKenzie (1978) for exponential drop in heat flow from syn to post-rift phases and the guidelines of Allen and Allen (2013) for average heat flow in active syn-rifting phases, post-rifting thermal subsidence, and compressional uplifts, while the mean present-day heat flow in the study area was inferred from Morgan and Swanbf (1978) and Mohamed et al. (2015). After iterating multiple runs of models to fine-tune the heat flow and achieve a good calibration, the following heat flows are assigned; 80 mW/m^2 for the Albian rifting, 45 mW/m^2 for the Late Cretaceous-Paleocene tectonic uplift, 64 mW/m^2 for the Miocene thermal uplift, and 62 mW/m^2 for the present-day heat flow (Fig. 9).

The Paleo water depth (PWD) was estimated based on the interpreted depositional environments of different rock units from previous sedimentological and paleontological studies (e.g. El Beialy et al., 2011; Salem and Sehim, 2017; Tahoun et al., 2017; Farouk et al., 2018; Shehata et al., 2018a, 2019; Ibrahim et al., 2020; Mahfouz et al., 2020). The Sediment-Water Interface Temperature (SWIT) was calculated using the global mean temperature at sea level for latitudes of 28° and 29°, Northern Africa, based on Wygrala (1989).

4.3.2. Burial History

Figure 10 portrays the burial history curve with temperatures overlay of Tareef-1X well and shows four alternating episodes of deposition and erosion linked with tectonic/thermal subsidence and uplift events: The Albian rifting phase, the Late Cretaceous- Paleocene tectonic uplift, the Eocene tectonic subsidence, and the Miocene thermal uplift. These episodes are interrupted by an erosional/non-depositional hiatus event during the Late Eocene-Oligocene time. Sedimentation was initiated during the Albian syn-rift phase with low burial rates of about 33 m/My, followed by rapid thermal subsidence accompanied by relatively moderate average sedimentation rates of around 117 m/My during the post-rift period until the Late Cretaceous, where an erosional uplift occurred and culminated through the entire Paleocene resulting in the removal of some parts of the Khoman Formation. Subsidence had resumed during the Eocene due to extensional tectonics with elevated average sedimentation rates of approximately 145 m/My, which resulted in a maximum burial depth of 3060 m. The Late Eocene-Oligocene hiatus is followed by the Miocene thermal uplift that lasted till the present and led to significant erosion from the Apollonia Formation. A maximum bottom temperature of 125 ℃ was reached at about 23 Ma in response to the maximum burial during the Eocene and the elevated heat flow associated with the thermal uplift of the Red Sea pre-rifting phase.

4.3.3. Thermal History

The thermal maturity history (Fig. 11) indicates that the Abu Roash "F" source rock has entered the early mature stage (0.55 - 0.7 $\%R_o$) and commenced generating oil during the Late Eocene (35 Ma) at depth of around 2400 m and has not reached the peak oil window till present. Initiation of hydrocarbon generation within the source rock was triggered by the extensive sedimentation during the Early to Middle Eocene resulting in maximum burial and temperatures.

Model calibration (Fig. 10 and 11) was achieved by the best fit between measured and predicted temperatures and vitrinite reflectance modeled according to Sweeney and Burnham (1990). The model was calibrated using 400 and 200 m of erosion from Apollonia and Khoman formations, respectively. Note that the higher vitrinite values are selected for the best fit to account for any potential suppression effect on the sediment maturity associated with the lower values as shown in Figures 5. a and 8.

The quantity of generated hydrocarbons is strongly controlled by the type and concentration of present kerogen as well as the associated thermal maturity levels (Cooles et al., 1986). Transformation ratio expresses the amount of converted kerogen over the total amount of available kerogen (Dembicki, 2017) and can be used as an indicator for the oil generation of source rocks. The Abu Roash "F" source rock has a present-day transformation ratio of about 19 % (Fig. 12), which confirms that the effective oil generation peak has not yet reached.

4.4. Sensitivity Analysis

Due to the intrinsic uncertainties of basin modeling, sensitivity analysis presents a means to examine the influence of the input parameters and boundary conditions on the reconstruction of the burial and thermal histories and to test alternate modeling scenarios considering different geologic interpretations (Cao and Lerche, 1990; Thomsen, 1998; Hicks Jr. et al., 2012; Dembicki, 2017). The paleo water depth has a minor impact on the modeling routine because it does not affect the compaction (Wygrala, 1989); we focused the sensitivity analysis on the eroded thickness and heat flow for the sensitivity analysis because they may contribute to uncertainty.

Although the basin has experienced two erosional events during its tectonic evolution, we considered only the younger erosion from the Apollonia Formation for the sensitivity analysis because the older erosion from the Khoman Formation is overprinted by the later geological events from the Eocene to the present and, consequently, has no impact on thermal maturity.

To finely tune the estimated eroded thickness and to examine the impact of varying the amount of erosion and heat flow on the thermal maturity of the sedimentary succession, we simulated three scenarios following the procedure introduced by Grobe et al. (2015); The first scenario

(Fig. 13. a) was modeled using the assigned heat flow in Figure 9 with varying the amount of erosion (300-500 m). This scenario shows that 400 m of erosion from the Apollonia Formation is required for the best fit between the measured and predicted vitrinite reflectance data and indicates that as the amount of eroded thickness increases, the maturity levels increase as shown by shifting the modeled thermal profiles to higher values. The increase in maturity levels with increasing the magnitude of eroded sections can be attributed to the greater paleo burial depths the strata reached prior to the erosional uplift events. The second scenario (Fig. 13. b) was simulated using a constant amount of erosion of 400 m with various fixed heat flows (55-65 mW/m^2) only from the Paleocene to Recent, as changing the heat flow before this period has no significant impact on the thermal maturity because this period has witnessed the tectonic uplift that was culminated during the Paleocene followed by the Eocene extensive overburden sedimentation and the subsequent Miocene thermal uplift. We found that higher heat flows resulted in higher thermal maturity levels indicating the same impact as the eroded thickness and in this case, the best fit is achieved with a heat flow of 60 mW/m^2.

The third scenario (Fig. 13. c) was performed using a fixed heat flow of 65 mW/m^2 representing the average global heat flow (Allen and Allen, 2013) with varying the amount of erosion (100-300 m). In this scenario, 200 m of erosion is sufficient for model calibration, which is half of the amount of erosion in the previous scenarios. In this case, the decrease in the amount of erosion is compensated by the higher heat flow during the Late Cretaceous-Paleocene tectonic uplift, which emphasizes the mutual impact of the heat flow and the amount of erosion on the thermal maturity, hence underlying the significance of a reasonable and realistic adjustment of both parameters as a prerequisite for a more reliable basin modeling.

Although the available composite reports of the studied wells in the East Beni Suef Basin indicate the absence of the Oligocene Dabaa Formation compared with the West Beni Suef Basin, we present another two possible scenarios of the basin models (Fig. 14) suggesting the deposition and later complete erosion of the Dabaa Formation compared with the reference model (Fig. 10 and 11). The first scenario proposed a complete erosion of the Dabaa Formation, while the second one was simulated by a combined erosion of the Dabaa and Apollonia formations, both scenarios were constructed using the same predefined heat flow (Fig. 9) with a slight decrease in the present-day heat flow from 62 to 60 mW/m^2.

The results of these scenarios demonstrate that 250 m representing a complete erosion of the Dabaa Formation or a combined erosion of 200 m and 100 m from the Dabaa and Apollonia formations, respectively, are required to accomplish the best fit curve. Also, Figure 14 clearly indicates that the required amount of erosion is strongly dependent on the eroded lithology that in turn affects the maturity levels, where the eroded thickness of shale is lower than the eroded thickness of limestone, this can be related to the different thermal properties of rocks like thermal conductivity and thermal heat capacity, as the thermal conductivity of shale is approximately half of that for limestone.

4.5. Comparison with the West Beni Suef Basin

Based on recently published literature on the geologic history of the Beni Suef Basin (e.g. Zahran et al., 2011; Abd El-Aal et al., 2015; El Batal et al., 2016; Abd El-Gawad et al., 2017; Elanbaawy et al., 2017; Salem and Sehim, 2017; Shehata et al., 2018a, 2018b, 2019, 2020, 2021; Sakran et al., 2019; Abdelbaset et al., 2020), there is a general consensus that the basin differs from the north Western Desert basins regarding the timing of rift inception that occurred during the Aptian/Albian time with Kharita Formation representing the oldest recorded deposits on the Pre-Cambrian basement.

Four published studies have focused on the construction of the burial and thermal history of the West Beni Suef Basin including Makky et al. (2014), Abd El-Gawad et al. (2017), Abdel-Fattah et al. (2017), and Edress et al. (2021), which are discussed briefly in the next section.

Makky et al. (2014) have assumed the deposition of a Jurassic succession and adopted the general stratigraphy of the northern Western Desert for the West Beni Suef Basin. Abd El-Gawad et al. (2017) have postulated a hiatus from the Late Eocene to the present, which in contrast with the recorded Late Eocene-Oligocene Dabaa Formation in the west Beni Suef Basin and incorporated an uplift during the beginning of the Upper Cretaceous, which is however inconsistent with the post-rift cooling subsidence of this time. Abdel-Fattah et al. (2017) have presumed the deposition of the pre-Kharita section of Alam El-Bueib Formation on the basement and subsequently suggested seven depositional and erosional episodes. A detailed comparison with the modeling results of Edress et al. (2021) is not possible because their input data and boundary conditions are not included in the publication. In contrast to our model, they assumed continuous subsidence during the Miocene thermal uplift of the Red Sea (Abdelbaset et al., 2020) thereby ignoring the impact of this significant tectonic event on organic matter maturation, which results in a much later (Early Miocene) onset of hydrocarbon generation compared to all other published hydrocarbon generation models and our model presented here.

Moreover, none of these published models have adjusted the heat flow history in context with the tectonic evolution of the basin, which plays a crucial role in the modeling process and output as discussed in the sensitivity analysis.

All these assumptions have resulted in uncertainties within the published models; in this study, we reconstructed the burial and thermal history of the West Beni Suef Basin according to the recently published tectonic and stratigraphic studies of the basin. We selected the Fayoum-1X well from the literature (Makky et al., 2014; Abdel-Fattah et al., 2017) as it contains more available data of the Lower Cretaceous section, where the top of the Lower Kharita Shale Member is picked approximately as the top of the Alam El-Bueib Formation in Abdel-Fattah et al. (2017) and is verified through gamma-ray log correlation with other wells in the study area from previous stratigraphic literature (Shehata et al., 2018a), then we assigned the absolute age, lithologic description, and geochemical analyses accordingly. For the Lower Kharita Shale source rock in the West Beni Suef basin, which includes terrestrial organofacies type DE (Abdelbaset et al., 2020), we applied the kinetic of Pepper and Corvi (1995)_TIIIH(DE).

We modeled the West Beni Suef Basin (Fig. 15-17) using almost the same heat flow of the East Beni Suef Basin for the Albian rifting and Late-Cretaceous-Paleocene uplift tectonics, while the heat flows for the Miocene thermal uplift and the present-day are 59 and 52 mW/m^2, respectively, as deduced from the best fit of model calibration. These lower heat flow values could be attributed to the presence of thick shale succession with lower thermal conductivity in the West Beni Suef Basin compared with the East Beni Suef Basin. Regarding the amount of eroded thickness, 500 m from the Dabaa Formation and 100 m from the Khoman Formation are required to explain the present levels of maturity.

Our results of the burial history of the West Beni Suef Basin reveal the same four alternating episodes of deposition and erosion as the East Beni Suef Basin without the Late Eocene-Oligocene hiatus event, where the basin has continued subsiding and resulted in the deposition of the Dabaa Formation (Fig. 15). The burial history curve illustrates major subsidence and high sedimentation rates of about 210 m/My during the Albian time associated with the deposition of the syn-rift Kharita Formation. This stage was followed by the post-rift phase, which is characterized by gentle subsidence and moderate sedimentation rates of about 97 m/My and lasted till the end of the Cretaceous prior to the first tectonic uplift event that culminated during the Paleocene time and resulted in erosion of Khoman Formation. From the Eocene to the end of the Paleogene period, increased tectonic subsidence has occurred with relatively low sedimentation rates of approximately 74 m/My. The last tectonic stage is represented by the Miocene thermal uplift (Abdelbaset et al., 2020), which led to a considerable erosion from the Dabaa Formation. The burial history of the West Beni Suef Basin shows that the sedimentation began earlier (Early Albian) and with higher rates compared with the East Beni Suef Basin. Regarding the sedimentation start, the paleo basement high as deduced from previous seismic interpretation studies (e.g. Zahran et al., 2011; Abd El-Aal et al., 2015; Salem and Sehim, 2017) has hindered the deposition of the Lower Kharita shales in the East Beni Suef Basin, thus caused a delay at the beginning of the deposition. The different rates of sedimentation could be attributed to various factors such as the amount of sediment supply from erosional catchment, climate, relief, different slopes along both sides of the basin, and /or lithology (Leeder et al., 1998).

A maximum temperature of 160 °C was reached at the maximum burial depth of 4000 m, which was triggered by the continued deposition by the end of the Oligocene coupled with the enhanced heat flow during the Miocene thermal uplift (Fig. 15). The thermal maturity model (Fig. 16) shows that the Abu Roash “F” source rock has entered the early mature stage of the oil window during the Early Oligocene (around 31 Ma) at a depth of 2150 m, where the peak oil window has not been reached yet. The Lower Kharita Shale source rock has initiated oil generation during the Cenomanian age (about 95 Ma) at a depth of 1600 m, entered the peak maturity stage during the Coniacian (88 Ma) at a depth of 2150 m, and the Late oil generation window during the Early Miocene (19 Ma) at depth 3500 m and has not reached the postmature stage until the present. These successive maturity levels are attributed to the integrated effects of the greater thicknesses of the overburden associated with the tectonic subsidence and the elevated heat flows during the Early Cretaceous rifting and the Miocene thermal uplift.

The transformation ratio of the Abu Roash “F” and the Lower Kharita source rocks at the present day is about 21 % and 70 % respectively (Fig. 17) indicating the presence of the Abu Roash “F” in the early generation stage, while the lower Kharita shale reached the late oil window.

4.6. Petroleum System of the Beni Suef Basin

A petroleum system offers a dynamic record of all essential geological elements and processes that drive hydrocarbons to accumulate (Hantschel and Kauerauf, 2009). These elements include: an active source rock, reservoir rock, seal rock, and overburden rocks, while the processes encompass: trap formation, hydrocarbon generation, migration, and accumulation (Magoon and Dow, 1994; Beaumont and Magoon, 1999).

Figure 18 summarizes the petroleum system analysis of the East Beni Suef Basin as a genetic relation in time between all involved elements and processes. Based on the results of the source rock evaluation, the Turonian Abu Roash "F" Member represents the main source rock. Reservoir rocks including sandstones of the Upper Cenomanian and the Coniacian Abu Roash "E" and "G" members and seal rocks represented by shales and carbonates of the Abu Roash "G" and "D" members are defined after Zahran et al. (2011). According to Abd El-Aal et al. (2015) and Salem and Sehim (2017), traps formed within the East Beni Suef Basin are structural traps in the form of three-way dip closures associated with the extensional faulted blocks and the anticlines related to the transtentional movements during the Late Cretaceous-Early Paleogene in response to the dextral motion of Africa relative to Eurasia. The timing of hydrocarbon generation, migration, and accumulation is determined based on the results of the thermal modeling from this study. With regard to the West Beni Suef Basin, we updated the events charts presented in Abdel-Fattah et al. (2017) and Sakran et al. (2019) in terms of the timing of the oil generation, migration, and accumulation and the critical moment in the view of our results as shown in Figure 19.

To present a complete picture of the Beni Suef Basin, Table 6 summarizes and compares the results of this work and previously published studies (Makky et al., 2014; El Batal et al., 2016; Abd El-Gawad et al., 2017; Abdel-Fattah et al., 2017; Sakran et al., 2019; Edress et al., 2021) on the source rock characteristics and thermal modeling results of both the East and West Beni Suef basins. The Abu Roash "F" Member, which is recorded throughout the entire Beni Suef Basin, displays compatible source characteristics of very good richness, oil-prone mainly type II kerogen, and marginal thermal maturity across both sides of the basin. It commenced oil generation during the Late Eocene and has not exceeded the early oil window yet. The Lower Kharita source rock is restricted to the West Beni Suef Basin and characterized by fair to good potential, gas-prone type III kerogen with late maturity levels. It has entered the early oil window during the Cenomanian, the peak oil window during the Coniacian, and the late oil window during the Early Miocene but has not reached the postmature stages yet.

5. Conclusions

Detailed source rock evaluation, basin modeling, and sensitivity analysis for the sedimentary succession of the East Beni Suef Basin were conducted, where the following findings can be concluded:

1. Three kerogen types can be distinguished: oil-prone type II kerogen in the Apollonia Formation and Abu Roash "F" Member, mixed type II/III kerogen in the Abu Roash "A" and "G" members, and gas-prone type III kerogen in the Abu Roash "E" Member and Bahariya Formation.
2. Kerogen data analysis reveals variation in the maceral composition of the sedimentary succession from liptinite to vitrinite with minor traces of inertinite, which reflects variations in the depositional conditions.
3. The Abu Roash "F" Member represents the main source rock exhibiting good to excellent source-potential, oil-prone type II kerogen, and immature to marginal thermal maturity levels.
4. The reconstructed burial history of the Beni Suef Basin shows four alternating depositional and erosional phases from the Late Cretaceous to Recent interrupted by an erosional/non-depositional hiatus period during the Late Eocene-Oligocene in the East Beni Suef Basin, while the West Beni Suef Basin has continued subsiding.

Sedimentation began later (Middle to Late Albian) with lower rates in the East Beni Suef Basin than in the West Beni Suef Basin (Early Albian).

5. The Abu Roash "F" source rock is in the early oil window in both sides of the basin, while the Lower Kharita source rock occurs only in the West Beni Suef Basin in the late oil window.
6. Based on basin model calibration, eroded thickness of 400 m from the Apollonia Formation and 500 m from the Dabaa Formation are estimated in the East and west Beni Suef basins, respectively.
7. We could not constrain the deposition of the Late Eocene-Oligocene Dabaa Formation within the East Beni Suef Basin compared with the western side of the basin, thus we suggested two additional possible scenarios of basin modeling concerning the deposition and later complete erosion of the Dabaa Formation.
8. Palynofacies and biomarker studies are highly recommended to determine the depositional environment of the Abu Roash "F" source rock and to precisely differentiate the oil-prone kerogen type.
9. Results of this work can serve as a basis for subsequent 2D and/or 3D basin modeling to further investigate the petroleum system evolution of the Beni Suef Basin.

Acknowledgments

We are grateful to the Egyptian General Petroleum Corporation (EGPC) in collaboration with the Qarun Petroleum Company for providing the available data and samples to conduct this research. We would like to express our great appreciation to the University of Potsdam for providing support and infrastructure. We are grateful to Schlumberger for having made available the software required to achieve the goals of this study. Special thanks to the sedimentary research group at the Institute of Geoscience, Potsdam University for their valuable feedback and discussion.

Funding Source Declaration

The researcher Ahmed Yousef Tawfik is funded by a full scholarship from the Ministry of Higher Education of the Arab Republic of Egypt.

References

Aabø, T.M., Hermanrud, C., 2019. Toward a global model for correction of bottomhole temperature data: Progress and limitations. Am. Assoc. Pet. Geol. Bull. 103, 139–155. https://doi.org/10.1306/0607181612117167

Abd El-Aal, M.H., Attia, T.E., Aboulmagd, M.A., 2015. Structural Analysis and Tectonic Evolution based on Seismic Interpretation in East of Nile valley, BeniSuef basin, Egypt. IOSR J. Appl. Geol. Geophys. Ver. I 3, 2321–990. https://doi.org/10.9790/0990-03515160

Abd El-Gawad, E.A., Lotfy, M.M., El-Sherbiny, M., Agam, A., 2017. Source rock evaluation of Abu Roash (F) member in Beni Suef concession, Western Desert, Egypt. Egypt. J. Appl. Geophys. 16, 1–20.

Abdel-Fattah, M.I., Attia, T.E., Abd El-Aal, M.H., Hanafy, M.I., 2021. Seismic interpretation of the Late Albian-Early Cenomanian Bahariya reservoirs of Burg El Arab oil field for tectonic evaluation: a case study from Western Desert, Egypt. Arab. J. Geosci. 14, 1–11. https://doi.org/10.1007/S12517-021-06745-9/FIGURES/10

Abdel-Fattah, M.I., Pigott, J.D., Abd-Allah, Z.M., 2017. Integrative 1D-2D Basin Modeling of the Cretaceous Beni Suef basin, Western Desert, Egypt. J. Pet. Sci. Eng. 153, 297–313. https://doi.org/10.1016/j.petrol.2017.04.003

Abdel-Fattah, M.I., Pigott, J.D., El-Sadek, M.S., 2020. Integrated seismic attributes and stochastic inversion for reservoir characterization: Insights from Wadi field (NE Abu-Gharadig Basin, Egypt). J. African Earth Sci. 161, 14. https://doi.org/10.1016/J.JAFREARSCI.2019.103661

Abdelbaset, M., Gong, C., Bosworth, B., Versfelt, J., 2020. Egypt Beni Suef Basin Petroleum Systems from Oil Geochemistry and Basin Modeling, in: AAPG Hedberg Conference. pp. 1–2. https://doi.org/10.1306/11290Gong2020

Allen, P.A., Allen, J.R., 2013. Basin analysis: Principles and application to petroleum play assessment, Third Edit. ed. John Wiley & Sons.

Badalini, G., Redfern, J., Carr, I.D., 2002. A Synthesis of Current Understanding of The Structural Evolution of North Africa. J. Pet. Geol. 25, 249–258. https://doi.org/10.1111/J.1747-5457.2002.TB00008.X

Beaumont, E.A., Magoon, L.B., 1999. Petroleum Systems, in: Beaumont, E.A., Foster, N.H. (Eds.), Treatise of Petroleum Geology / Handbook of Petroleum Geology: Exploring for Oil and Gas Traps. The American Association of Petroleum Geologistq, p. 34. https://doi.org/10.1306/trhbk624c3

Bosworth, W., Stockli, D.F., 2016. Early magmatism in the greater Red Sea rift : timing and significance. Can. J. Earth Sci. 53, 1158–1176. https://doi.org/10.1139/cjes-2016-0019

Cao, S., Lerche, I., 1990. Basin modelling: Applications of sensitivity analysis. J. Pet. Sci. Eng. 4, 83–104. https://doi.org/10.1016/0920-4105(90)90018-X

Cooles, G.P., Mackenzie, A.S., Quigley, T.M., 1986. Calculation of petroleum masses generated and expelled from source rocks. Org. Geochem. 10, 235–245. https://doi.org/10.1016/0146-6380(86)90026-4

Corcoran, D. V., Doré, A.G., 2005. A review of techniques for the estimation of magnitude and timing of exhumation in offshore basins. Earth-Science Rev. 72, 129–168. https://doi.org/10.1016/j.earscirev.2005.05.003

Dembicki, H., 2017. Practical Petroleum Geochemistry for Exploration and Production, Elsevier Inc. Candice Janco. https://doi.org/10.1016/c2014-0-03244-3

Dembicki, H., 2009. Three common source rock evaluation errors made by geologists during prospect or play appraisals. Am. Assoc. Pet. Geol. Bull. 93, 341–356. https://doi.org/10.1306/10230808076

Deming, D., 1989. Application of bottom-hole temperature corrections in geothermal studies. Geothermics 18, 775–786. https://doi.org/10.1016/0375-6505(89)90106-5

Dolson, J.C., Atta, M., Blanchard, D., Sehim, A., Villinski, J., Loutit, T., Romine, K., 2014. Egypt's future petroleum resources: A revised look into the 21st century, Memoir 106: Petroleum Systems of the Tethyan Region. https://doi.org/10.1306/13431856m106713

Dolson, J.C., Shann, M. V., Matbouly, S., Harwood, C., Rashed, R., Hammouda, H., 2001. The petroleum potential of Egypt, in: Downey, M.W., Threet, J.C., Morgan, W.A. (Eds.), Petroleum Provinces of the Twenty-First Century. AAPG Memoir 74, pp. 453–482. https://doi.org/10.1306/m74775c23

Dow, W.G., 1977. Kerogen studies and geological interpretations. J. Geochemical Explor. 7, 79–99. https://doi.org/10.1016/0375-6742(77)90078-4

Edress, N.A.A., Darwish, S., Ismail, A., 2021. Geochemical characterization of the source rock intervals, Beni-Suef Basin, West Nile Valley, Egypt. Open Geosci. 13, 1536–1551. https://doi.org/10.1515/GEO-2020-0306/HTML

EGPC, 1992. Western Desert, Oil and Gas Fields (a comprehensive overview). Egyptian General Petroleum Corporation In 11th EGPC Petrol. Explor. and Prod. Conf. Cairo.

El-Soughier, M.I., Deaf, A.S., Mahmoud, M.S., 2014. Palynostratigraphy and palaeoenvironmental significance of the Cretaceous palynomorphs in the Qattara Rim-1X well, North Western Desert, Egypt. Arab. J. Geosci. 7, 3051–3068. https://doi.org/10.1007/s12517-013-0954-x

El-Werr, A., Shebl, A., El-Rawy, A., Al-Gundor, N., 2017. Pre-drill pore pressure prediction using seismic velocities for prospect areas at Beni Suef Oil Field, Western Desert, Egypt. J. Pet. Explor. Prod. Technol. 7, 1011–1021. https://doi.org/10.1007/s13202-017-0359-6

El Batal, A., Abdelwahab, O., Clerk, C., Abdou, M., 2016. Effect of Lacustrine Petroleum Source Rock on the distribution of the Recoverable Oil Accumulations Beni-Suef Basin , in: 13th Mediterranean Offshore Conference and Exhibition (MOC), ALEX., EGYPT. pp. 1–15.

El Beialy, S.Y., El-Soughier, M.I., Abdel Mohsen, S., El Atfy, H.S., 2011. Palynostratigraphy and paleoenvironmental significance of the Cretaceous succession in the Gebel Rissu-1 well, north Western Desert, Egypt. J. African Earth Sci. 59, 215–226. https://doi.org/10.1016/j.jafrearsci.2010.10.007

El Beialy, S.Y., El Atfy, H.S., Zavada, M.S., El Khoriby, E.M., Abu-Zied, R.H., 2010. Palynological, palynofacies, paleoenvironmental and organic geochemical studies on the Upper Cretaceous succession of the GPTSW-7 well, North Western Desert, Egypt. Mar. Pet. Geol. 27, 370–385. https://doi.org/10.1016/j.marpetgeo.2009.10.006

El Diasty, W.S., Moldowan, J.M., 2013. The Western Desert versus Nile Delta: A comparative molecular biomarker study. Mar. Pet. Geol. 46, 319–334. https://doi.org/10.1016/J.MARPETGEO.2013.07.003

El Nady, M.M., 2008. Biomarkers Assessment of Crude Oils and Extracts from Jurassic-Cretaceous Rocks, North Qattara Depression, North Western Desert, Egypt. Pet. Sci. Technol. 26, 1063–1082. https://doi.org/10.1080/10916460701208496

Elanbaawy, M.I., Amin, A.T., Osman, O.A., 2017. Reservoir quality of Upper " G " Member sandstone of Abu Roash. IOSR J. Appl. Geol. Geophys. 5, 10–23. https://doi.org/10.9790/0837-0506011023

Evans, T.R., Coleman, N.C., 1974. North Sea geothermal gradients. Nature 247, 28–30. https://doi.org/10.1038/247028a0

Farouk, S., Ismail, A., Abd El-Rauf, I., Tawfik, M., 2018. Foraminiferal palaeobathymetry and depositional sequences of the subsurface Eocene Apollonia Formation in North Western Desert, Egypt. Palaeobio Palaeoenv 98, 403–429. https://doi.org/10.1007/s12549-017-0312-1

Ghassal, B.I., Littke, R., El Atfy, H., Sindern, S., Scholtysik, G., El Beialy, S., El Khoriby, E., 2018. Source rock potential and depositional environment of Upper Cretaceous sedimentary rocks, Abu Gharadig Basin, Western Desert, Egypt: An integrated palynological, organic and inorganic geochemical study. Int. J. Coal Geol. 186, 14–40. https://doi.org/10.1016/J.COAL.2017.11.018

Goutorbe, B., Lucazeau, F., Bonneville, A., 2007. Comparison of several BHT correction methods: A case study on an Australian data set. Geophys. J. Int. 170, 913–922. https://doi.org/10.1111/j.1365-246X.2007.03403.x

Grobe, A., Littke, R., Sachse, V., Leythaeuser, D., 2015. Burial history and thermal maturity of Mesozoic rocks of the Dolomites, Northern Italy. Swiss J. Geosci. 108, 253–271. https://doi.org/10.1007/s00015-015-0191-2

Guiraud, R., 1998. Mesozoic rifting and basin inversion along the northern African Tethyan margin: an overview, in: MAC- GREGOR, D.S., MOODY, R.T.J., CLARK-LOWES, D.D. (Eds.), Petroleum Geology of North Africa. Geological Society of London, Special Publications, pp. 217–229. https://doi.org/10.1144/GSL.SP.1998.132.01.13

Hantar, G., 1990. North Western Desert, in: Said, R. (Ed.), The Geology of Egypt. A.A. Balkema/Rotterdam/Bookfield, pp. 293–319. https://doi.org/10.1201/9780203736678-15

Hantschel, T., Kauerauf, A.I., 2009. Fundamentals of basin and petroleum systems modeling, Springer Berlin Heidelberg. https://doi.org/10.1007/978-3-540-72318-9

Hawkesworth, C., Kelley, S., Turner, S., Roex, A.L.E., Storey, B., 1999. Mantle processes during Gondwana break-up and dispersal. J. African Earth Sci. 28, 239–261. https://doi.org/10.1016/S0899-5362(99)00026-3

Hermanrud, C., Caot, S., Lerche, I., 1990. Estimates of virgin rock temperature derived from BHT measurements: Bias and error. GEOPHYSICS 55. https://doi.org/10.1190/1.1442908

Hicks Jr., P.J., Fraticelli, C.M., Shosa, J.D., Hardy, M.J., Townsley, M.B., 2012. Identifying and Quantifying Significant Uncertainties in Basin Modeling, in: Peters, K.E., Curry, D.J., Kacewicz, M. (Eds.), Basin Modeling: New Horizons in Research and Applications. AAPG Hedberg Series, pp. 207–219. https://doi.org/10.1306/13311437H41527

Ibrahim, M.I.A., Tahoun, S.S., Zobaa, M.K., Oboh-Ikuenobe, F.E., Kholeif, S.E., 2020. Late Cretaceous palynology and paleoenvironment of the Razzak-3 well, North Western Desert, Egypt. Arab. J. Geosci. 13, 23. https://doi.org/10.1007/s12517-020-05705-z

Jones, R.W., 1984. Comparison of Carbonate and Shale Source Rocks: ABSTRACT, in: Palacas, J.G. (Ed.), Petroleum Geochemistry and Source Rock Potential of Carbonate Rocks. American Association of Petroleum Geologists, Tulsa, Okla. U.S.A, pp. 163–180. https://doi.org/10.1306/AD460EA4-16F7-11D7-8645000102C1865D

Keeley, M.L., Massoud, M.S., 1998. Tectonic controls on the petroleum geology of NE Africa, in: MAC- GREGOR, D.S., MOODY, R.T.J., CLARK-LOWES, D.D. (Eds.), Petroleum Geology of North Africa. Geological Society of London, Special Publications, pp. 265–281. https://doi.org/doi.org/10.1144/GSL.SP.1998.132.01.15

Khalil, A., Abdel Hafeez, T.H., Saleh, H.S., Mohamed, W.H., 2016. Inferring the subsurface basement depth and the structural trends as deduced from aeromagnetic data at West Beni Suef area, Western Desert, Egypt. NRIAG J. Astron. Geophys. 5, 380–392. https://doi.org/10.1016/j.nrjag.2016.08.001

Leeder, M.R., Harris, T., Kirkby, M.J., 1998. Sediment supply and climate change: implications for basin stratigraphy. Basin Res. 10, 7–18.

Macgregor, D.S., Moody, R.T.J., 1998. Mesozoic and Cenozoic petroleum systems of North Africa, in: MAC- GREGOR, D.S., MOODY, R.T.J., CLARK-LOWES, D.D. (Eds.), Petroleum Geology of North Africa. Geological Society of London, Special Publications, pp. 201–216. https://doi.org/10.1144/GSL.SP.1998.132.01.12

Magoon, L.B., Dow, W.G., 1994. The petroleum system from source to trap. Am. Assoc. Pet. Geol. Mem. 60 3–24.

Mahfouz, K.H., El-Sheikh, I., Obaidalla, N.A., Shreif, A., 2020. New insights into stratigraphy and paleoenvironment of the Upper Cretaceous–Eocene succession, Farafra Oasis, Western Desert, Egypt. J. African Earth Sci. 104096, 46. https://doi.org/10.1016/j.jafrearsci.2020.104096

Makky, A.F., El Sayed, M.I., Abu El-Ata, A.S., Abd El-Gaied, I.M., Abdel-Fattah, M.I., Abd-Allah, Z.M., 2014. Source rock evaluation of some upper and lower Cretaceous sequences, West Beni Suef Concession, Western Desert, Egypt. Egypt. J. Pet. 23, 135–149. https://doi.org/10.1016/j.ejpe.2014.02.016

McCarthy, K., Niemann, M., Palmowski, D., Peters, K., Stankiewicz, A., 2011. Basic

Petroleum Geochemistry for Source Rock Evaluation. Oilf. Rev. 23, 32–43.

McKenzie, D., 1978. Some remarks on the development of sedimentary basins. Earth Planet. Sci. Lett. 40, 25–32. https://doi.org/10.1016/0012-821X(78)90071-7

Merrill, R.K., 1991. Source and migration processes and evaluation techniques. American Association of Petroleum Geologists, Tulsa, Okla. U.S.A. https://doi.org/10.1306/TRHBK543

Meshref, W.M., 1990. Tectonic Framework of Egypt, in: Said, R. (Ed.), The Geology of Egypt. A.A. Balkema/Rotterdam/Bookfield, pp. 113-156.

Mohamed, H.S., Abdel Zaher, M., Senosy, M.M., 2015. Geothermal Gradients in the North Western Desert, Egypt as Deduced from Bottom-Hole Temperature and Aerogravity Data, in: Proceedings World Geothermal Congress. Melbourne, Australia, p. 4.

Mohamed, O., Mahdy, F., Tahoun, S.S., 2020. Palynofacies analysis and source rock evaluation of the Upper Cretaceous-Oligocene succession in the Drazia-1 well, Alamein Basin, Egypt. Arab. J. Geosci. 13, 1–17. https://doi.org/10.1007/S12517-020-06174-0/FIGURES/9

Morgan, P., Swanbf, C.A., 1978. Heat Flow and the Geothermal Potential of Egypt. Pageoph. 17, 213–226.

Moustafa, A.R., 2008. Mesozoic-Cenozoic Basin Evolution in the Northern Western Desert of Egypt. Geol. East Libya 3, 29–46.

Nemec, M., Colley, G., 1998. Abstract: Qarun and Beni Suef Oil Discoveries - Western Desert, Egypt, in: Houston Geological Society Bulletin. pp. 11–11. https://doi.org/10.1306/00aa9124-1730-11d7-8645000102c1865d

Norton, P., 1967. Rock stratigraphic nomenclature of the Western Desert Egypt., Int. Report of GPC, Cairo, Egypt.

Pepper, A.S., Corvi, P.J., 1995. Simple kinetic models of petroleum formation. Part I: oil and gas generation from kerogen. Mar. Pet. Geol. 12, 291–319. https://doi.org/10.1016/0264-8172(95)98381-E

Peters, K.E., 1986. Guidelines for Evaluating Petroleum Source Rock Using Programmed Pyrolysis. Am. Assoc. Pet. Geol. Bull. 70, 318–329. https://doi.org/10.1306/94885688-1704-11D7-8645000102C1865D

Peters, K.E., Cassa, M.R., 1994. Applied Source Rock Geochemistry, in: In: Magoon, L.B., Dow, W.G. (Eds.), The Petroleum System – From Source to Trap. American Association of Petroleum Geologists Memoir Vol. 60, pp. 93–120.

Peters, K.E., Nelson, P.H., 2012. Criteria to Determine Borehole Formation Temperatures for Calibration of Basin and Petroleum System Models, in: Analyzing the Thermal History of Sedimentary Basins: Methods and Case Studies. SEPM Special Publication No. 103, pp. 5–15. https://doi.org/10.2110/sepmsp.103.005

Peters, K.E., Walters, C.C., Moldowan, J.M., 2005. The biomarker guide (Vol. 1), 2nd ed. Cambridge University Press, Cambridge.

Poelchau, H.S., 2001. Modeling an Exhumed Basin: A Method for Estimating Eroded Overburden, Natural Resources Research.

Rabeh, T., Ali, K., Bedair, S., Sadik, M.A., Ismail, A., 2019. Exploration and evaluation of potential groundwater aquifers and subsurface structures at Beni Suef area in southern Egypt. J. African Earth Sci. 151, 9–17. https://doi.org/10.1016/j.jafrearsci.2018.11.025

Saber, S.G., Salama, Y.F., 2017. Facies analysis and sequence stratigraphy of the Eocene successions, east Beni Suef area, eastern Desert, Egypt. J. African Earth Sci. 135, 173–185. https://doi.org/10.1016/j.jafrearsci.2017.09.006

Said, R., 1962. The Geology of Egypt. Elsevier Publ. Co.Amsterdam. Oxford and New York, Amsterdam. Oxford and New York.

Sakran, S., Shehata, A.A., Osman, O., El-Sherbiny, M., 2019. Superposed tectonic regimes in west Beni Suef basin, Nile Valley, Egypt: Implications to source rock maturation and hydrocarbon entrapment. J. African Earth Sci. 154, 1–19. https://doi.org/10.1016/j.jafrearsci.2019.03.010

Salem, E., Sehim, A., 2017. Structural imaging of the East Beni Sueif Basin, north eastern Desert, Egypt. J. African Earth Sci. 136, 109–118.

https://doi.org/10.1016/j.jafrearsci.2017.05.009
Shehata, A.A., El Fawal, F.M., Abdel Aal, M.H., Aboulmagd, M.A., 2018b. Seismic Facies Interpretations and Depositional Sequences of the Cretaceous Sediments in Beni Suef Basin, Nile Valley, Egypt. IOSR J. Appl. Geol. Geophys. 6, 57–69. https://doi.org/10.9790/0990-0606025769
Shehata, A.A., El Fawal, F.M., Ito, M., Abdel Aal, M.H., Sarhan, M.A., 2019. Cenomanian–Turonian depositional history of a post–Gondwana rift succession in the West Beni Suef Basin, Egypt. J. African Earth Sci. 150, 783–798. https://doi.org/10.1016/j.jafrearsci.2018.10.006
Shehata, A.A., El Fawal, F.M., Ito, M., Abdel Aal, M.H., Sarhan, M.A., 2018a. Sequence stratigraphic evolution of the syn-rift Early Cretaceous sediments, West Beni Suef Basin, the Western Desert of Egypt with remarks on its hydrocarbon accumulations. Arab. J. Geosci. 11. https://doi.org/10.1007/s12517-018-3688-y
Shehata, A.A., El Fawal, F.M., Ito, M., Aboulmagd, M.A., Brooks, H.L., 2020. Senonian platform-to-slope evolution in the tectonically-influenced Syrian Arc sedimentary belt: Beni Suef Basin, Egypt. J. African Earth Sci. 170, 103934. https://doi.org/10.1016/J.JAFREARSCI.2020.103934
Shehata, A.A., Osman, O.A., Nabawy, B.S., 2021. Neural network application to petrophysical and lithofacies analysis based on multi-scale data: An integrated study using conventional well log, core and borehole image data. J. Nat. Gas Sci. Eng. 93, 18. https://doi.org/10.1016/J.JNGSE.2021.104015
Smith, A.G., 1971. Alpine Deformation and the Oceanic Areas of the Tethys, Mediterranean, and Atlantic. GSA Bull. 82, 2039–2070. https://doi.org/10.1130/0016-7606(1971)82[2039:adatoa]2.0.co;2
Storey, B.C., 1996. Microplates and mantle plumes in Antarctica. Terra Antart. 3, 91–102.
Storey, B.C., 1995. The role of mantle plumes in continental breakup: Case histories from Gondwanaland. Nature 377, 301–308. https://doi.org/10.1038/377301a0
Sweeney, J.J., Burnham, A.K., 1990. Evaluation of a simple model of vitrinite reflectance based on chemical kinetics. Am. Assoc. Pet. Geol. Bull. 74, 1559–1570. https://doi.org/10.1306/0C9B251F-1710-11D7-8645000102C1865D
Tahoun, S.S., Deaf, A.S., Mansour, A., 2017. Palynological, palaeoenvironmental and sequence stratigraphical analyses of a Turonian-Coniacian sequence, Beni Suef Basin, Eastern Desert, Egypt: Implication of Pediastrum rhythmic signature. Mar. Pet. Geol. 88, 871–887. https://doi.org/10.1016/j.marpetgeo.2017.09.026
Tawadros, E., 2011. Geology of North Africa, Expanded a. ed. CRC Press/Balkema, Boca Raton, FL. https://doi.org/10.1201/b11419
Thomsen, R.O., 1998. Aspects of applied basin modelling: sensitivyt analysis and scientific risk, in: Dueppenbecker, S.J., Iliffe, J.E. (Eds.), Basin Modelling: Practice and Progress. Geological Society, London, Special Publications, London, pp. 209–221. https://doi.org/10.1144/GSL.SP.1998.141.01.13
Tissot, B.P., Welte, D.H., 1984. Petroleum Formation and Occurrence, 2nd ed. Springer Berlin Heidelberg. https://doi.org/10.1007/978-3-642-87813-8
Waples, D.W., 1985. Geochemistry in Petroleum Exploration, 1st ed. Springer Netherlands, Dordrecht. https://doi.org/10.1007/978-94-009-5436-6
Waples, D.W., Ramly, M., 2001. A statistical method for correcting log-derived temperatures. Pet. Geosci. 7, 231–240. https://doi.org/10.1144/petgeo.7.3.231
Wilson, M., Guiraud, R., Moreau, C., Bellion, Y.J.C., 1998. Late Permian to Recent magmatic activity on the African-Arabian margin of Tethys, in: MAC- GREGOR, D.S., MOODY, R.T.J., CLARK-LOWES, D.D. (Eds.), Petroleum Geology of North Africa. Geological Society, London, Special Publications, pp. 231–263. https://doi.org/10.1144/GSL.SP.1998.132.01.14
Wood, B.G.M., 2015. Rethinking post-Hercynian basin development: Eastern Mediterranean Region. GeoArabia 20, 175–224.
Wygrala, B., 1989. Integrated Study of an Oil field in the Southern Po Basin, Northern Italy. Kernforschungsanlage Jülich GmbH, Zentralbiliothek, Verlag.

Zahran, H., Abu Elyazid, K., Mohamad, M., 2011. Beni Suef Basin the Key for Exploration Future Success in Upper Egypt *, in: AAPG Annual Convention And Exhibition, Houston, Texas, USA.

Tables Captions

Table 1 Rock-Eval pyrolysis and TOC data for the Apollonia Formation in Gharibon-1X, Gharibon NE-1X, and Tareef-1X Wells, East Beni Suef basin, Egypt.
Table 2 Rock-Eval pyrolysis and TOC data for the Abu Roash Formation in Gharibon-1X, Gharibon NE-1X, and Tareef-1X Wells, East Beni Suef basin, Egypt.
Table 3 Rock-Eval pyrolysis and TOC data for the Bahariya Formation in Gharibon-1X, Gharibon NE-1X, and Tareef-1X Wells, East Beni Suef basin, Egypt.
Table 4 Vitrinite reflectance, Thermal Alteration Index, and petrographic kerogen typing of the Upper Cretaceous-Eocene Section in Gharibone-1X, Gharibon NE-1x, and Tareef-1X wells, East Beni Suef basin, Egypt.
Table 5 Input data used for the burial and thermal history modeling for the Tareef-1X well, East Beni Suef Basin.
Table 6 Summary and comparison of the source rocks characteristics throughout the entire Beni Suef Basin based on the results of this study and previous literature.

Figures Captions

Fig. 1 Location Map showing the Beni Suef Basin bisected by the Nile Valley into West and East of Nile provinces and main sedimentary basins in the Western Desert and Upper Egypt (modified after Dolson et al., 2001; Bosworth et al., 2008; Moustafa, 2008), Beni Suef Concession added after Zahran et al. (2011).

Fig. 2 General stratigraphic column of the East Beni Suef Basin (as indicated by the penetrated lithologies of the Gharibon-1X and Tareef-1X wells) in correlation with the West Beni Suef Basin (modified after Zahran et al., 2011; Salem and Sehim, 2017).

Fig. 3 Plot of TOC versus remaining hydrocarbon potential (S2) indicating source rock richness of the Upper Cretaceous-Eocene sediments, East Beni Suef Basin, Egypt.

Fig. 4 Modified van-Krevelen diagram showing kerogen types of the Upper Cretaceous-Eocene sediments, East Beni Suef Basin, Egypt.

Fig. 5 Thermal maturity profiles of the Upper Cretaceous-Eocene sediments from (a) vitrinite reflectance and (b) Thermal Alteration Index data showing immature to marginally mature stages and a strong correlation between %Ro and TAI. The red oval indicates suppressed %Ro or caved sediments.

Fig. 6 Plot of PI versus T_{max} revealing the maturation and nature of hydrocarbons of the Upper Cretaceous-Eocene sediments, East Beni Suef Basin, Egypt.

Fig. 7 Ternary plot of the maceral composition showing hydrocarbon phases of the Upper Cretaceous-Eocene sediments, East Beni Suef Basin, Egypt.

Fig. 8 Erosion estimation at the top of Apollonia Formation using Dow's method (1977).

Fig. 9 Boundary Conditions for the thermal history of the Tareef-1X well including paleo water depth (PWD), sediment water interface temperature (SWIT), and heat flow (HF).

Fig. 10 Burial history with temperature overlay and model calibration by measured temperatures for Tareef-1X well, East Beni Suef Basin.

Fig. 11 Thermal maturity history with hydrocarbon zones overlay and model calibration by measured vitrinite reflectance for Tareef-1X well, East Beni Suef Basin.

Fig. 12 Transformation ratio of the Abu Roash "F" source rock, Tareef-1X well.

Fig. 13 Sensitivity analysis of the eroded thickness and heat flow. (a) using the predefined heat flow with different amounts of erosion, (b) using a constant eroded thickness of 400 m with different fixed heat flows, and (c) using a constant heat flow of 65 mW/m^2 with various amounts of erosion.

Fig. 14 Possible scenarios of thermal maturity modeling concerning erosion from the Apollonia and Dabaa formations.

Fig. 15 Burial history with temperature overlay and model calibration by measured temperatures for Fayoum-1X well, West Beni Suef Basin.

Fig. 16 Thermal maturity history with hydrocarbon zones overlay and model calibration by measured vitrinite reflectance for Fayoum-1X well, West Beni Suef Basin.

Fig. 17 Transformation ratios of the Abu Roash "F" and Lower Kharita Shale source rocks, Fayoum-1X well, West Beni Suef Basin.

Fig. 18 Petroleum system events chart depicting the essential geological elements and processes of the East Beni Suef Basin.

Fig. 19 Petroleum system events chart depicting the essential geological elements and processes of the West Beni Suef Basin (modified and updated after Abdel-Fattah et al., 2017; Sakran et al., 2019).

Table 1 Rock-Eval pyrolysis and TOC data for the Apollonia Formation in Gharibon-1X, Gharibon NE-1X, and Tareef-1X Wells, East Beni Suef basin, Egypt.

Well	Depth (m)	TOC (wt|%)	S1 (mg HC/g rock)	S2 (mg HC/g rock)	S3 (mg CO_2/g rock)	Tmax (°C)	HI (mg HC/g TOC)	OI (mg CO_2/g TOC)	PI S1(/S1+S2)
Gharibon-1X	262.13	0.53	0.41	3.28	0.29	422	619	55	0.11
	365.76	1.05	0.55	9.33	0.31	419	889	30	0.06
	441.96	0.49							
	554.74	0.31							
	646.18	0.28							
	728.47	0.35							
	819.91	0.39							
	938.78	0.79	0.47	5.25	0.18	424	665	23	0.08
	1021.08	0.44							
	1103.38	0.43							
	1194.82	0.49							
	1249.68	0.57	0.36	2.36	0.22	422	414	39	0.13
	1258.82	0.93	0.91	4.82	0.26	420	518	28	0.16
	1267.97	1.67	0.48	8.81	0.21	420	528	13	0.05
	1295.40	0.39							
	1304.54	0.49							
Gharibon NE-1X	306.32	0.78	0.18	2.78	0.58	422	358	75	0.06
	388.62	0.82	0.24	4.48	0.28	428	547	34	0.05
	480.06	1.47	0.47	8.98	0.26	423	613	18	0.05
	571.50	0.87	0.35	5.19	0.23	426	597	26	0.06
	662.94	0.36							
	754.38	0.59	0.46	3.41	0.28	424	582	48	0.12
	845.82	0.46							
	937.26	1.72	0.39	10.40	0.27	424	606	16	0.04
	1028.70	1.30	0.34	7.66	0.34	427	592	26	0.04
	1120.14	0.77	0.29	4.65	0.27	430	607	35	0.06
	1211.58	0.69	0.25	3.86	0.28	428	559	41	0.06
	1303.02	0.70	0.19	3.35	0.29	425	480	42	0.05
Tareef-1X	306.32	2.77	0.87	18.3	0.6	420	660	22	0.05
	361.19	2.23	0.69	13.71	0.39	421	616	18	0.05
	425.20	1.24	0.4	7.5	0.3	423	604	24	0.05
	480.06	0.55	0.28	3.09	0.04	420	560	7	0.08
	544.07	0.65	0.31	4.17	0.02	425	646	3	0.07
	608.08	0.2							
	662.94	0.45							
	726.95	0.19							
	790.96	0.34							
	845.82	0.48							
	909.83	0.36							
	973.84	0.31							
	1028.70	0.4							
	1092.71	0.35							
	1156.72	0.35							

1211.58	0.68	0.62	4.69	0.28	427	692	41	0.12
1275.59	2.08	0.67	10.47	0.02	426	505	1	0.06

Table 2 Rock-Eval pyrolysis and TOC data for the Abu Roash Formation in Gharibon-1X, Gharibon NE-1X, and Tareef-1X Wells, East Beni Suef basin, Egypt.

Well Name	Member	Depth (m)	TOC (wt|%)	S1 (mg HC/g rock)	S2 (mg HC/g rock)	S3 (mg CO_2/g rock)	T_{max} (°C)	HI (mg HC/g TOC)	OI (mg CO_2/g TOC)	PI S1(/S1+S2)
Gharibon-1X	**Abu Roash "A"**	1499.62	1.34	0.59	8.81	1.15	424	657	86	0.06
		1554.48	1.54	0.45	6.30	0.89	428	409	58	0.07
		1612.39	0.65	0.38	2.53	0.86	430	389	132	0.13
Gharibon NE-1X	**Abu Roash "A"**	1552.96	0.70	0.15	2.90	0.20	428	415	29	0.05
		1568.20	0.78	0.15	3.18	0.22	429	406	28	0.05
		1583.44	2.02	0.25	7.93	0.87	434	393	43	0.03
		1598.68	1.06	0.13	1.42	1.08	435	134	102	0.08
		1613.92	1.24	0.20	4.10	0.88	437	330	71	0.05
		1629.16	1.37	0.23	4.24	0.99	436	310	72	0.05
		1644.40	0.99	0.26	3.93	0.81	437	399	82	0.06
		1659.64	0.38							
Tareef-1X	**Abu Roash "A"**	1461.52	1.07	0.27	5.63	0.03	432	527	3	0.05
		1476.76	1.67	0.66	9.68	1.98	428	581	119	0.06
		1492.00	1.43	0.58	7.51	1.38	428	524	96	0.07
		1507.24	0.59	0.19	2.63	1.28	431	444	216	0.07
		1522.48	0.61	0.23	2.8	1.68	432	462	277	0.08
		1537.72	1.5	0.26	5.27	1.32	435	351	88	0.05
		1552.96	1.05	0.24	1.47	1.8	436	140	172	0.14
		1568.20	1.07	0.18	2.96	1.25	437	276	116	0.06
		1583.44	0.85	0.17	2.54	0.98	438	300	116	0.06
		1598.68	0.57	0.15	1.23	1.08	436	214	188	0.11
		1613.92	0.3							
Gharibon-1X	**Abu Roash "E"**	1990.34	0.58	0.34	1.20	0.57	310	207	98	0.22
		2036.06	1.63	0.60	3.02	1.60	430	185	98	0.17
		2042.16	1.76	0.58	3.09	1.77	432	176	101	0.16
		2048.26	1.78	0.87	4.53	1.55	431	254	87	0.16
Gharibon NE-1X	**Abu Roash "E"**	1918.72	1.48	0.26	2.25	0.64	439	152	43	0.10
		1933.96	1.00	0.23	1.14	0.61	438	114	61	0.17
		1949.20	2.06	0.19	2.23	0.41	438	108	20	0.08
		1964.44	0.85	0.13	0.71	0.52	439	83	61	0.15
		1979.68	0.54	0.09	0.31	0.92	436	58	172	0.23
		1994.92	0.22							
		2010.16	0.68	0.18	1.23	0.67	437	182	99	0.13
Tareef-1X	**Abu Roash "E"**	1873.00	4.99	0.81	12.52	0.5	437	251	10	0.06

		1888.24	0.77	0.17	0.74	0.29	443	96	38	0.19
		1903.48	2.71	0.64	5.02	1.01	438	185	37	0.11
		1918.72	0.8	0.21	0.82	0.97	441	102	121	0.2
		1933.96	2	0.27	3.05	0.6	441	152	30	0.08
		1949.20	0.41							
		1964.44	0.41							
		1979.68	0.67	0.11	0.58	0.99	438	86	148	0.16
		1982.72	0.97	0.15	1.17	1.21	441	120	124	0.11
		1985.77	1.27	0.25	2.87	0.88	439	227	70	0.08
		1988.82	1.21	0.36	2.83	1.21	438	234	100	0.11
Gharibon-1X	**Abu Roash "F"**	2054.35	1.43	1.11	8.07	0.98	430	564	69	0.12
		2060.45	4.02	4.23	27.91	0.89	425	694	22	0.13
		2066.54	2.99	2.11	18.73	1.28	424	626	43	0.10
		2072.64	2.59	2.08	18.46	0.88	431	713	34	0.10
Gharibon NE-1X	**Abu Roash "F"**	2016.25	3.99	3.50	25.40	0.58	429	637	15	0.12
		2022.35	3.53	3.16	22.65	0.71	432	642	20	0.12
		2028.44	3.35	2.75	20.54	0.49	432	613	15	0.12
		2034.54	3.23	1.80	14.92	1.65	431	462	51	0.11
Tareef-1X	**Abu Roash "F"**	1991.87	1.04	0.77	3.55	1.34	434	341	129	0.18
		1994.92	1.43	0.39	3.74	1.35	437	262	94	0.09
		1997.96	2.07	1.47	9.86	1.51	435	476	73	0.13
		2001.01	3.66	3.13	19.37	0.96	435	530	26	0.14
		2004.06	3.66	3.61	20.56	1.18	436	561	32	0.15
		2007.11	3.37	3.29	19.3	1.34	435	573	40	0.15
		2010.16	3.44	3.32	19.64	1.41	435	571	41	0.14
Gharibon-1X	**Abu Roash "G"**	2078.74	1.08	0.37	2.36	1.16	431	219	107	0.14
		2087.88	1.05	0.34	1.19	1.07	425	113	102	0.22
		2103.12	0.71	0.32	1.11	1.04	274	156	146	0.22
		2118.36	0.76	0.95	1.81	0.77	384	238	101	0.34
		2142.74	0.98	0.42	1.33	1.27	274	136	130	0.24
		2176.27	1.00	0.47	1.59	1.02	344	159	102	0.23
		2197.61	0.90	0.43	1.64	1.03	331	182	114	0.21
		2206.75	0.90	0.43	1.30	1.02	305	144	113	0.25
		2264.66	0.54	0.22	1.12	0.66	435	207	122	0.16
Gharibon NE-1X	**Abu Roash "G"**	2043.68	2.52	1.51	11.67	1.11	432	464	44	0.11
		2052.83	2.76	1.35	12.82	1.25	433	465	45	0.10
		2061.97	1.38	0.39	4.23	0.90	431	307	65	0.08
		2071.12	1.53	0.36	5.20	0.72	431	340	47	0.06
		2080.26	0.24							
		2089.40	0.38							
		2098.55	0.90	0.24	1.01	1.15	434	112	127	0.19
		2107.69	0.69	0.10	0.54	0.67	432	79	98	0.16
		2116.84	0.90	0.15	1.07	1.18	435	119	131	0.12

		2125.98	0.61	0.18	1.21	0.56	437	198	92	0.13
		2135.12	0.35							
		2144.27	0.29							
		2153.41	0.52	0.11	0.29	0.89	433	56	171	0.28
		2162.56	0.41							
		2171.70	0.57	0.16	1.06	0.70	441	185	122	0.13
		2180.84	1.27	0.48	3.01	0.60	435	237	47	0.14
		2189.99	0.74	0.22	1.65	0.26	441	223	35	0.12
		2199.13	0.59	0.17	1.23	0.53	443	207	89	0.12
		2208.28	0.54	0.14	0.80	0.53	440	148	98	0.15
		2217.42	0.21							
		2226.56	0.25							
Tareef-1X	**Abu Roash "G"**	2019.30	2.44	2.07	12.02	1.48	434	493	61	0.15
		2028.44	0.82	0.52	1.95	1.61	434	238	197	0.21
		2037.59	0.74	0.23	1.22	1.2	435	164	162	0.16
		2046.73	0.42							
		2055.88	0.2							
		2065.02	0.33							
		2074.16	0.29							
		2083.31	0.39							
		2092.45	0.48							
		2101.60	0.39							
		2110.74	0.81	0.36	1.17	0.84	441	144	104	0.24
		2119.88	0.65	0.17	0.81	0.42	439	125	65	0.17
		2129.03	0.6	0.1	0.72	1.01	439	120	168	0.12
		2138.17	0.3							
		2147.32	0.3							
		2156.46	0.59	0.13	0.79	0.96	440	133	162	0.14
		2165.60	1.3	0.3	3.36	0.9	445	258	69	0.08
		2174.75	0.73	0.17	1.22	0.82	443	168	113	0.12
		2183.89	0.61	0.13	0.77	1.58	441	127	261	0.14
		2193.04	0.51	0.17	0.76	1.1	442	148	214	0.18
		2202.18	0.27							
		2211.32	0.21							
		2220.47	0.41							

Table 3 Rock-Eval pyrolysis and TOC data for the Bahariya Formation in Gharibon-1X, Gharibon NE-1X, and Tareef-1X Wells, East Beni Suef basin, Egypt.

Well Name	Depth (m)	TOC (wt|%)	S1 (mg HC/g rock)	S2 (mg HC/g rock)	S3 (mg CO_2/g rock)	T_{max} (°C)	HI (mg HC/g TOC)	OI (mg CO_2/g TOC)	PI S1(/S1+S2)
Gharibon-1X	2307.34	0.83	0.42	1.43	0.58	368	172	70	0.23
	2350.01	2.25	0.83	4.01	0.86	439	178	38	0.17
	2386.58	1.43	0.58	2.91	1.86	438	203	130	0.17
	2462.78	0.74	0.67	2.12	1.62	404	286	219	0.24

Gharibon NE-1X	2238.76	1.56	0.47	3.90	0.46	443	250	29	0.11
	2247.90	0.57	0.16	0.94	0.44	442	164	77	0.15
	2257.04	0.29							
	2269.24	0.58	0.14	0.72	0.87	443	125	151	0.16
	2281.43	1.55	0.44	3.02	0.76	442	195	49	0.13
	2287.52	1.24	0.29	2.15	1.42	443	173	114	0.12
	2296.67	1.22	0.27	2.17	0.84	442	178	69	0.11
	2327.15	1.79	0.40	2.85	1.68	441	160	94	0.12
	2336.29	1.07	0.33	1.74	0.85	442	162	79	0.16
	2357.63	1.72	0.72	3.71	0.89	440	216	52	0.16
	2369.82	2.11	0.74	4.43	0.73	442	210	35	0.14
	2391.16	0.22							
	2403.35	0.12							
	2418.59	0.15							
	2427.73	0.23							
	2503.93	0.25							
Tareef-1X	2229.61	0.42							
	2235.71	0.41							
	2241.80	0.55	0.09	0.13	0.97	440	24	176	0.41
	2269.24	0.96	0.34	1.79	1.18	446	187	123	0.16
	2281.43	1.15	0.38	1.84	0.95	444	160	82	0.17
	2299.72	0.87	0.29	1.25	0.53	445	143	61	0.19
	2311.91	1.36	0.41	1.95	1.07	443	143	79	0.17
	2330.20	1.69	0.6	2.81	0.39	442	166	23	0.18
	2375.92	0.61	0.16	0.79	0.59	442	130	97	0.17
	2388.11	0.5	0.15	0.54	0.41	442	109	83	0.22
	2442.97	0.49							
	2449.07	0.27							
	2470.40	0.41							

Table 4 Vitrinite reflectance, Thermal Alteration Index, and petrographic kerogen typing of the Upper Cretaceous-Eocene Section in Gharibone-1X, Gharibon NE-1x, and Tareef-1X wells, East Beni Suef basin, Egypt.

Well Name	Formation	Depth (m)	%Ro	TAI	Macerals Composition		
					Liptinite (%)	Inertinite (%)	Vitrinite (%)
Gharibon-1X	**Apollonia**	1255.78		2	100	0	0
	Abu Roash "A"	1496.57		2	100	0	0
		1609.34		1.9	95	0	5
	Abu Roash "C"	1825.75	0.62		40	5	55
	Abu Roash "E"	1987.30	0.64		20	5	75
		2039.11	0.71	2.7	50	0	50
	Abu Roash "F"	2057.40		2	100	0	0
	Abu Roash "G"	2075.69		2	70	5	25

		2194.56		2.6	80	0	20
	Bahariya	2346.96		2	50	10	40
		2459.74		2	40	5	55
Gharibon NE-1X	**Apollonia**	480.06	0.39	2.35	95	0	5
		937.26	0.41	2.45	95	0	5
	Abu Roash "A"	1583.44	0.51	2.55	90	0	10
		1629.16	0.51	2.55	80	5	15
	Abu Roash "C"	1751.08	0.58	2.55	15	5	80
		1827.28	0.62	2.55	10	5	85
	Abu Roash "E"	1918.72	0.57	2.55	15	5	80
	Abu Roash "F"	2016.25	0.46	2.55	95	0	5
	Abu Roash "G"	2061.97	0.6	2.55	65	5	30
		2116.84	0.62	2.45	70	5	25
		2180.84	0.49	2.55	25	5	70
	Bahariya	2238.76	0.5	2.55	20	5	75
		2281.43	0.54	2.55	15	5	80
		2327.15	0.54	2.55	15	5	80
		2369.82	0.54	2.55	25	5	70
		2503.93	0.42	2.55	80	5	15
Tareef-1X	**Apollonia**	1275.59	0.47	2.45	95	0	5
	Abu Roash "A"	1461.52	0.49	2.45	95	0	5
		1537.72	0.56	2.55	80	5	15
	Abu Roash "C"	1690.12	0.6	2.55	25	5	70
		1781.56	0.62	2.55	30	5	65
	Abu Roash "E"	1873.00	0.57	2.55	20	5	75
		1933.96	0.58	2.55	20	5	75
		1985.77	0.65	2.65	35	5	60
	Abu Roash "F"	2004.06		2.55	95	0	5
	Abu Roash "G"	2110.74	0.57	2.55	30	5	65
		2165.60	0.52	2.55	55	10	35
	Bahariya	2269.24	0.56	2.55	25	5	70
		2281.43	0.6	2.65	30	5	65
		2330.20	0.58	2.65	20	5	75
		2388.11	0.6	2.65	20	15	65

Table 5 Input data used for the burial and thermal history modeling for the Tareef-1X well, East Beni Suef Basin.

Formation/Event	Present thickness (m)	Eroded thickness (m)	Age (Ma) From	To	Lithology
Apollonia-Erosion		400	23.70	0	
Dabaa-Hiatus			37.20	23.70	
Apollonia	1327		56.00	37.20	Limestone

Khoman-Erosion		200	66.00	56.00	
Khoman	125		83.60	66.00	Chalk
Abu Roash "A"	171		86.30	83.60	Limestone + Shale + Sandstone
Abu Roash "B"	54		89.80	86.30	Limestone + Siltstone + Sandstone
Abu Roash "C"	110		90.45	89.80	Siltstone + Limestone + Sandstone + Shale
Abu Roash "D"	83		90.90	90.45	Limestone + Siltstone + Shale
Abu Roash "E"	123		92.70	90.90	Shale + Siltstone + Sandstone + Limestone
Abu Roash "F"	25		93.90	92.70	Argillaceous Limestone
U. Abu Roash "G"	93		95.25	93.90	Shale + Limestone + Siltstone + Sandstone
M. Abu Roash "G"	53		95.85	95.25	Shale + Limestone + Siltstone + Sandstone
L. Abu Roash "G"	56		96.60	95.85	Limestone + Shale + Siltstone + Sandstone
Upper Bahariya	129		98.90	96.60	Siltstone + Sandstone + Shale
Lower Bahariya	141		100.50	98.90	Sandstone + Siltstone
Kharita	175		108.50	100.50	Sandstone + Siltstone
Basement	6		140.00	108.50	Granite

Table 6 Summary and comparison of the source rocks characteristics throughout the entire Beni Suef Basin based on the results of this study and previous literature.

Basin		Beni Suef Basin		
Sub-basin		West		East
Source Rock		Lower Kharita	A/R "F"	A/R "F"
Organic Richness		Fair to good[2,6]	Very good[1,3] Good to very good[2,4] Fair to very good[6]	Good to Excellent[7]
Kerogen Type		Mixed type II/III[2] Gas-prone type III[6]	Oil-prone type II[2,3] Oil-prone mixed type I/II[1,4] Oil-prone type II and II/III[6]	Oil-prone type II[7]
Thermal Maturity		Mature[5] Mature to postmature[2,6]	Immature[3] Immature to marginally mature[1,4,5] Marginally mature[2] Mature[6]	Immature to marginally mature[7]
Hydrocarbon Generation	Early stage	Cenomanian (97 Ma)[6] and (95 Ma)[7] Late Cretaceous[5]	Early Oligocene (30Ma)[4] and (31 Ma)[7] Middle Oligocene (28 Ma)[3] Late Oligocene (24 Ma)[1] Early Miocene (18 Ma)[6]	late Eocene (35 Ma)[7]

	Peak stage	Turonian (91 Ma)[6] Coniacian (88 Ma)[7] Late Cretaceous[5]	Late Miocene (8 Ma)[3] Not yet reached[1,4,6,7]	Not yet reached[7]
	Late stage	Late Paleocene (58 Ma)[6] Early Oligocene[5] Early Miocene (19 Ma)[7]	Not yet reached[1,3,4,6,7]	Not yet reached[7]
Transformation Ratio		70 %[7]	24 %[3] 16 %[4] 21 %[7]	19 %[7]

[1](Makky et al., 2014), [2](El Batal et al., 2016), [3](Abdel-Fattah et al., 2017), [4](Abd El-Gawad et al., 2017), [5](Sakran et al., 2019), [6](Edress et al., 2021), and [7](This work).

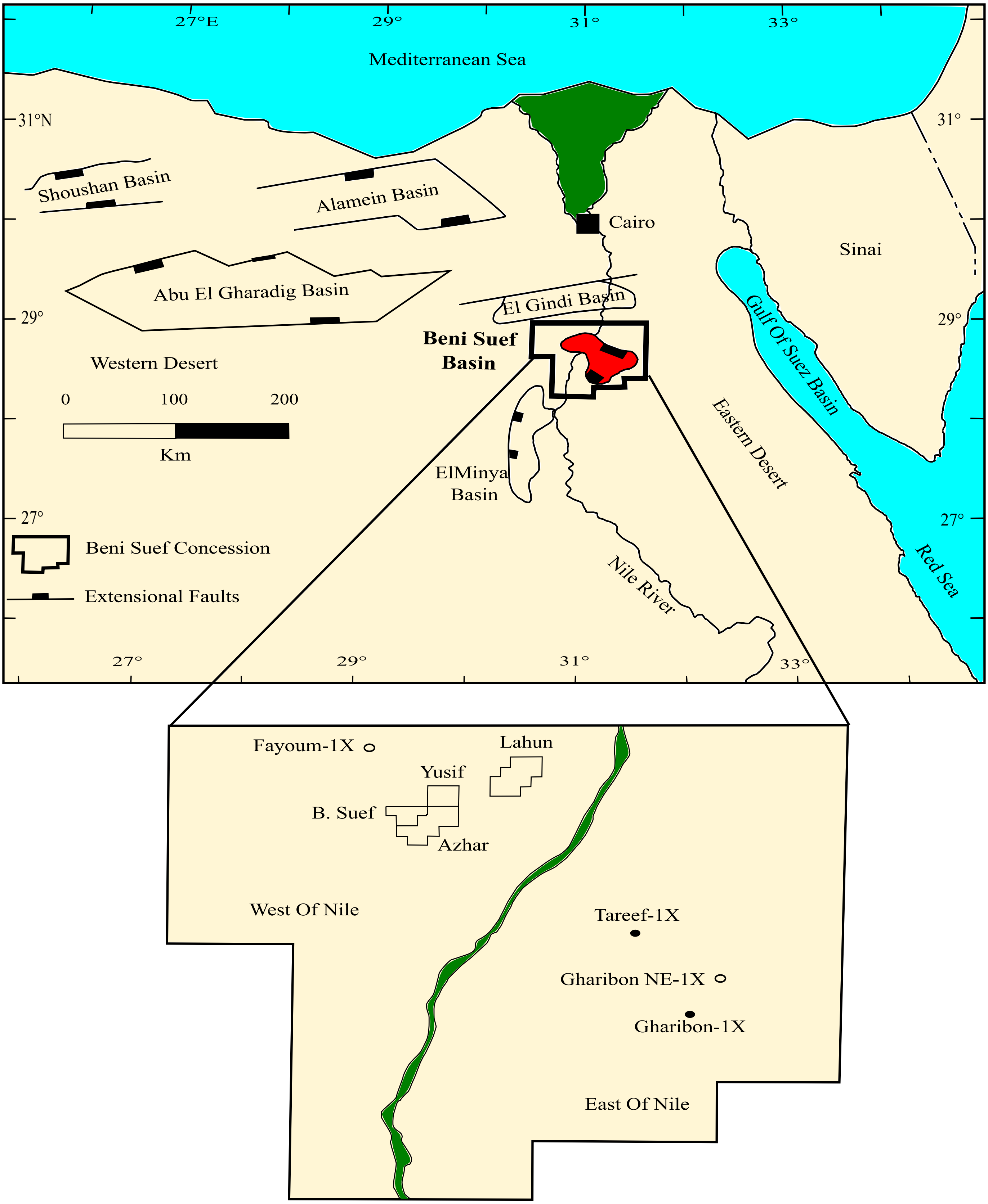
27°E
29°
31°
33°
Mediterranean Sea
31°N
31°
Shoushan Basin
Alamein Basin
Cairo
Sinai
Abu El Gharadig Basin
El Gindi Basin
29°
29°
Beni Suef Basin
Gulf Of Suez Basin
Western Desert
0
100
200
Km
Eastern Desert
ElMinya Basin
27°
27°
Beni Suef Concession
Red Sea
Nile River
Extensional Faults
27°
29°
31°
33°
Fayoum-1X
Lahun
Yusif
B. Suef
Azhar
West Of Nile
Tareef-1X
Gharibon NE-1X
Gharibon-1X
East Of Nile

Fig. 1

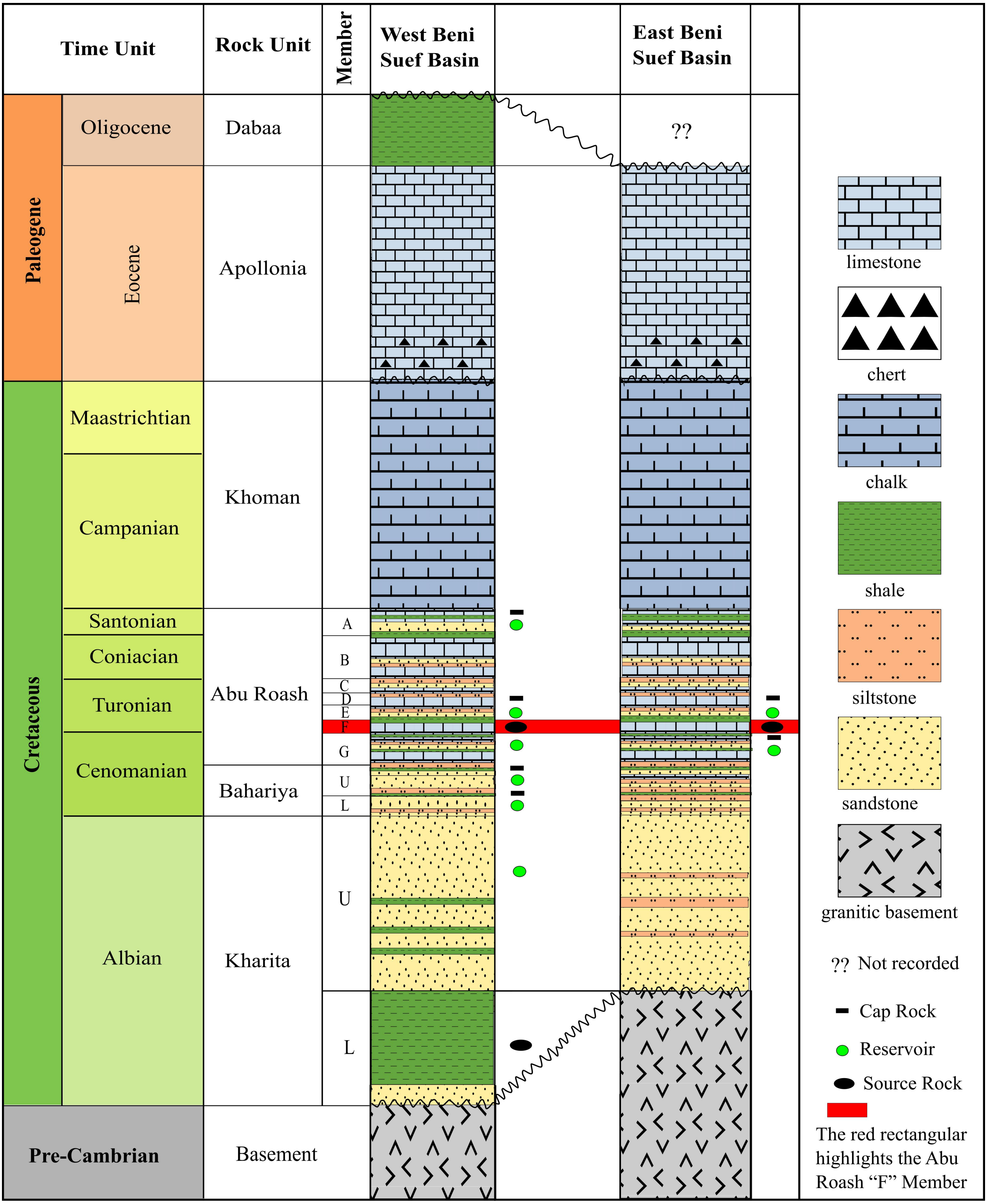
Time Unit
Rock Unit
Member
West Beni Suef Basin
East Beni Suef Basin
Paleogene
Oligocene
Eocene
Cretaceous
Maastrichtian
Campanian
Santonian
Coniacian
Turonian
Cenomanian
Albian
Pre-Cambrian
Dabaa
Apollonia
Khoman
Abu Roash
Bahariya
Kharita
Basement
A
B
C
D
E
F
G
U
L
U
L
??
limestone
chert
chalk
shale
siltstone
sandstone
granitic basement
?? Not recorded
Cap Rock
Reservoir
Source Rock
The red rectangular highlights the Abu Roash "F" Member

Fig. 2

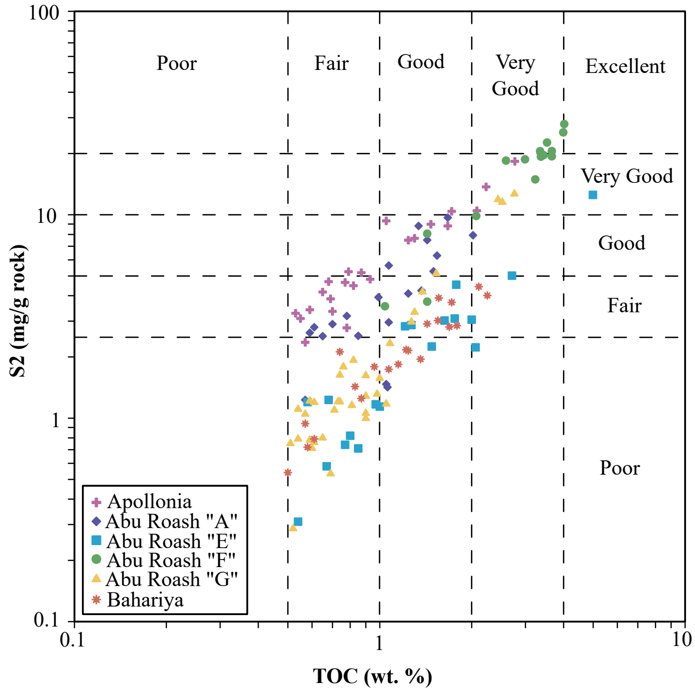
Poor
Fair
Good
Very Good
Excellent
Very Good
Good
Fair
Poor
100
10
1
0.1
0.1
1
10
S2 (mg/g rock)
TOC (wt. %)
Apollonia
Abu Roash "A"
Abu Roash "E"
Abu Roash "F"
Abu Roash "G"
Bahariya

Fig. 3

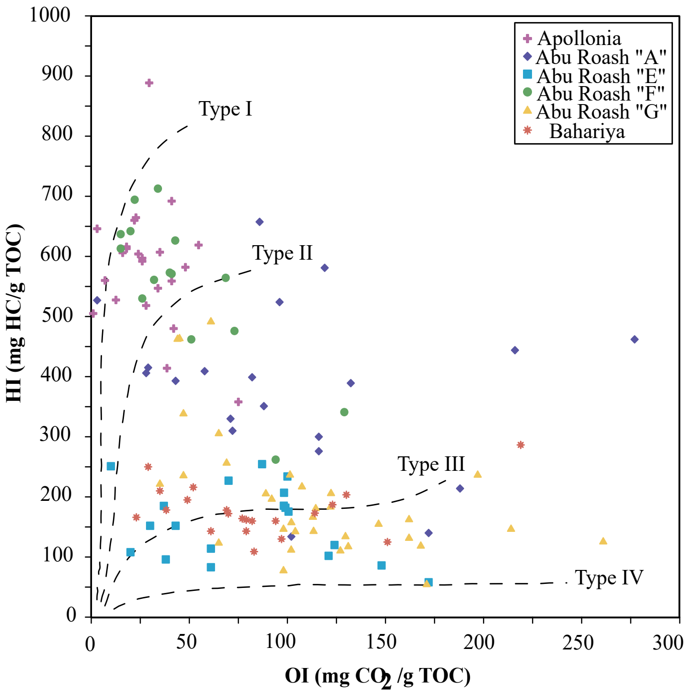

Apollonia
Abu Roash "A"
Abu Roash "E"
Abu Roash "F"
Abu Roash "G"
Bahariya
Type I
Type II
Type III
Type IV
HI (mg HC/g TOC)
OI (mg CO2 /g TOC)
0
100
200
300
400
500
600
700
800
900
1000
0
50
100
150
200
250
300

Fig. 4

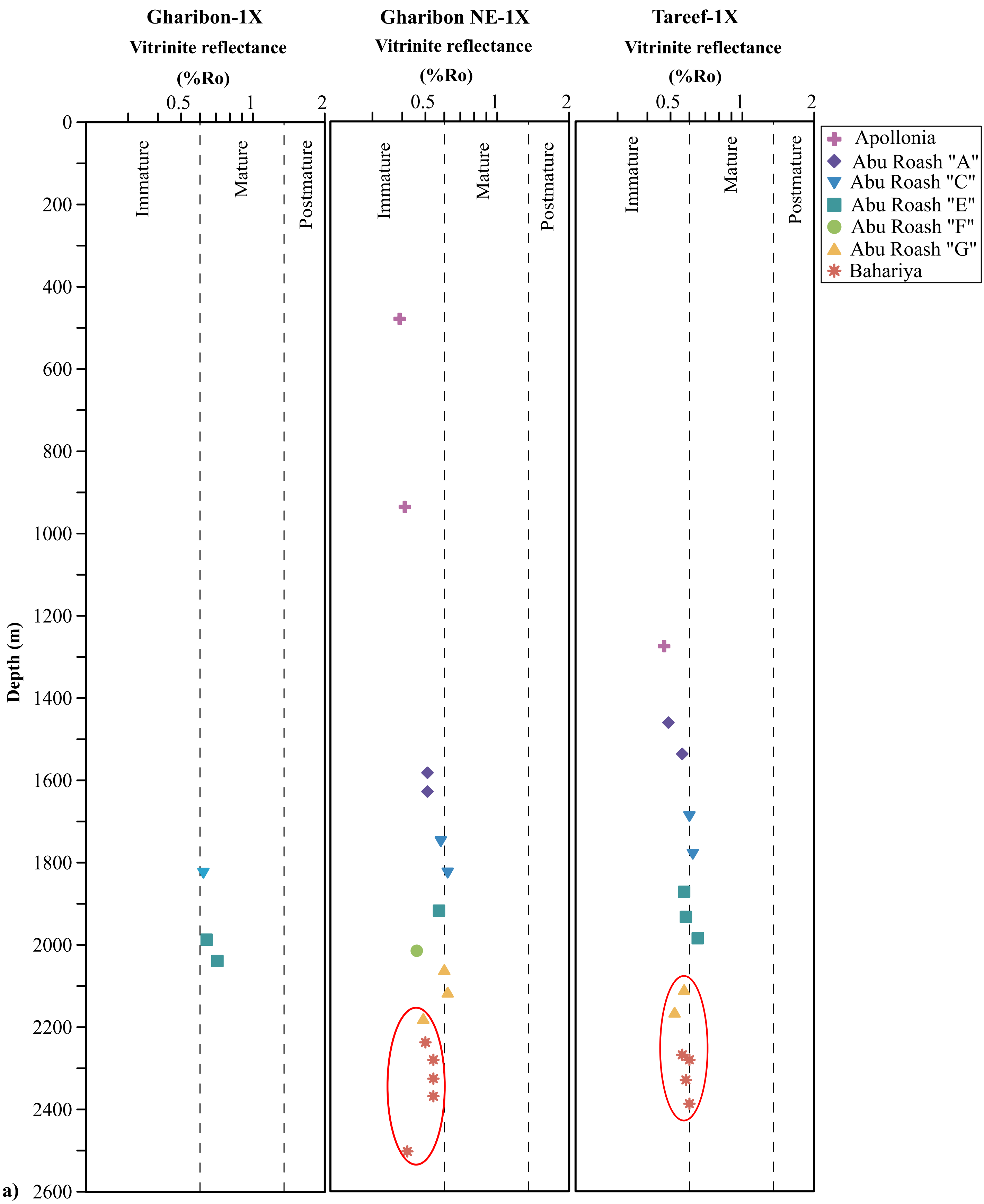
Gharibon-1X
Vitrinite reflectance
(%Ro)
Gharibon NE-1X
Vitrinite reflectance
(%Ro)
Tareef-1X
Vitrinite reflectance
(%Ro)
0.5
1
2
Immature
Mature
Postmature
Depth (m)
0
200
400
600
800
1000
1200
1400
1600
1800
2000
2200
2400
2600
a)
Apollonia
Abu Roash "A"
Abu Roash "C"
Abu Roash "E"
Abu Roash "F"
Abu Roash "G"
Bahariya

Fig. 5. a

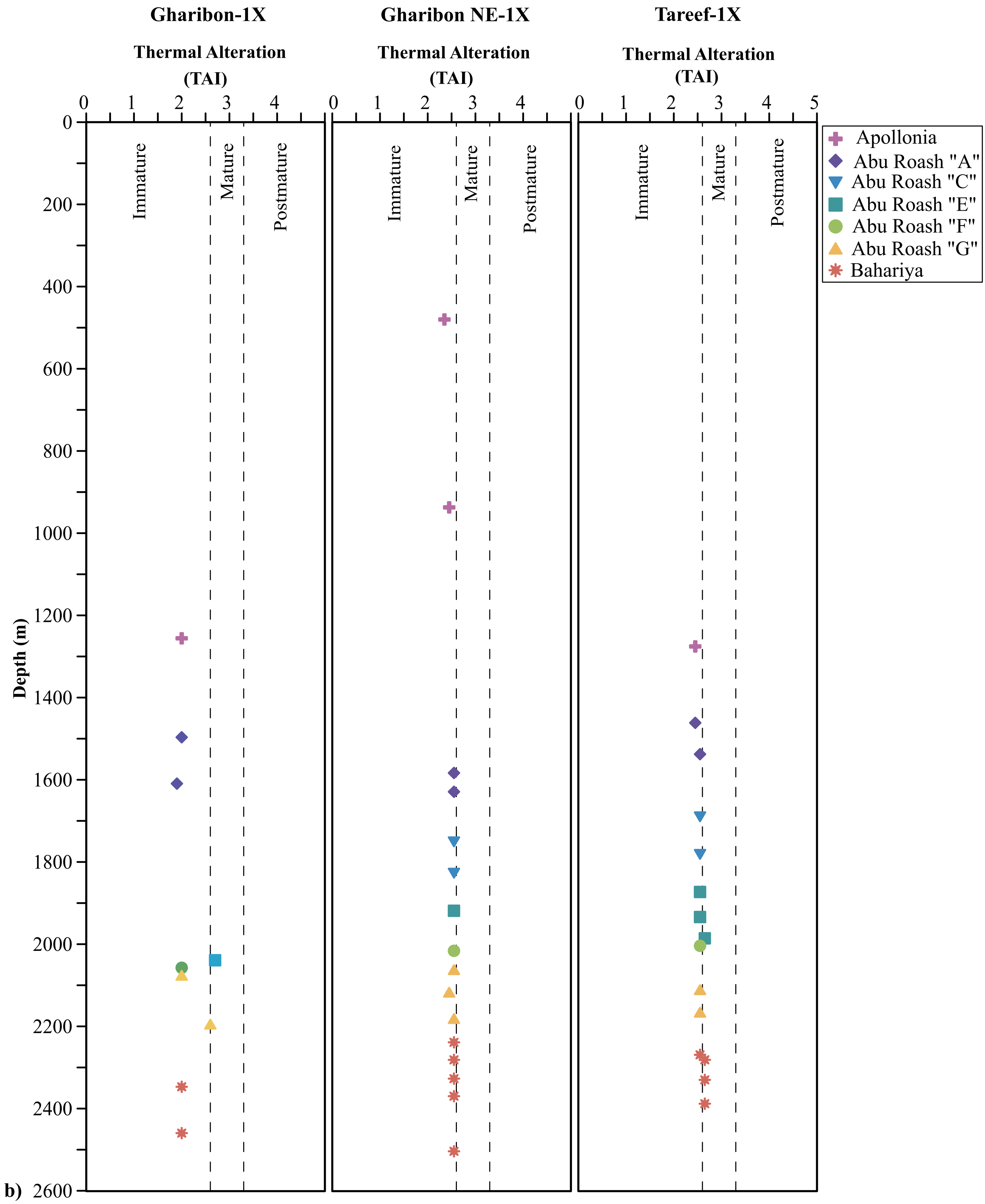
Gharibon-1X
Thermal Alteration
(TAI)
Gharibon NE-1X
Thermal Alteration
(TAI)
Tareef-1X
Thermal Alteration
(TAI)
Immature
Mature
Postmature
Depth (m)
b)
Apollonia
Abu Roash "A"
Abu Roash "C"
Abu Roash "E"
Abu Roash "F"
Abu Roash "G"
Bahariya

Fig. 5. b

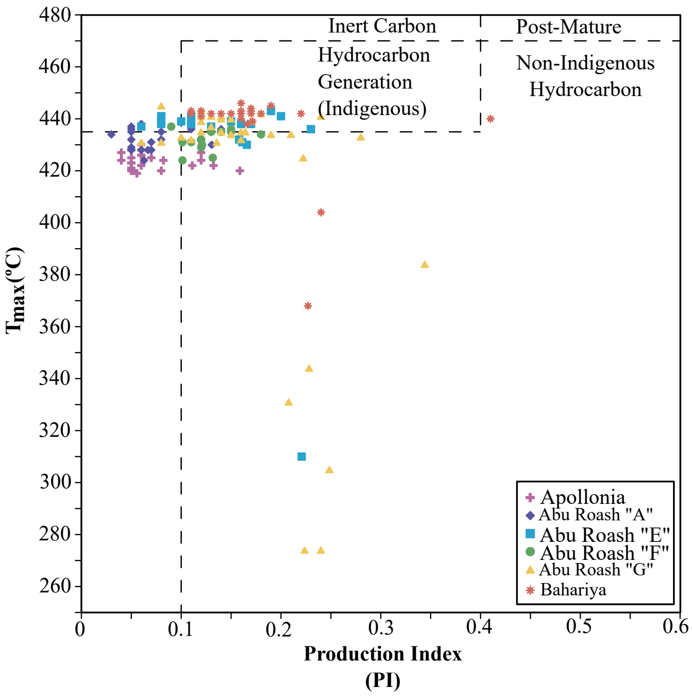
Inert Carbon
Post-Mature
Hydrocarbon
Generation
(Indigenous)
Non-Indigenous
Hydrocarbon
Apollonia
Abu Roash "A"
Abu Roash "E"
Abu Roash "F"
Abu Roash "G"
Bahariya
Tmax(ºC)
Production Index
(PI)

Fig. 6

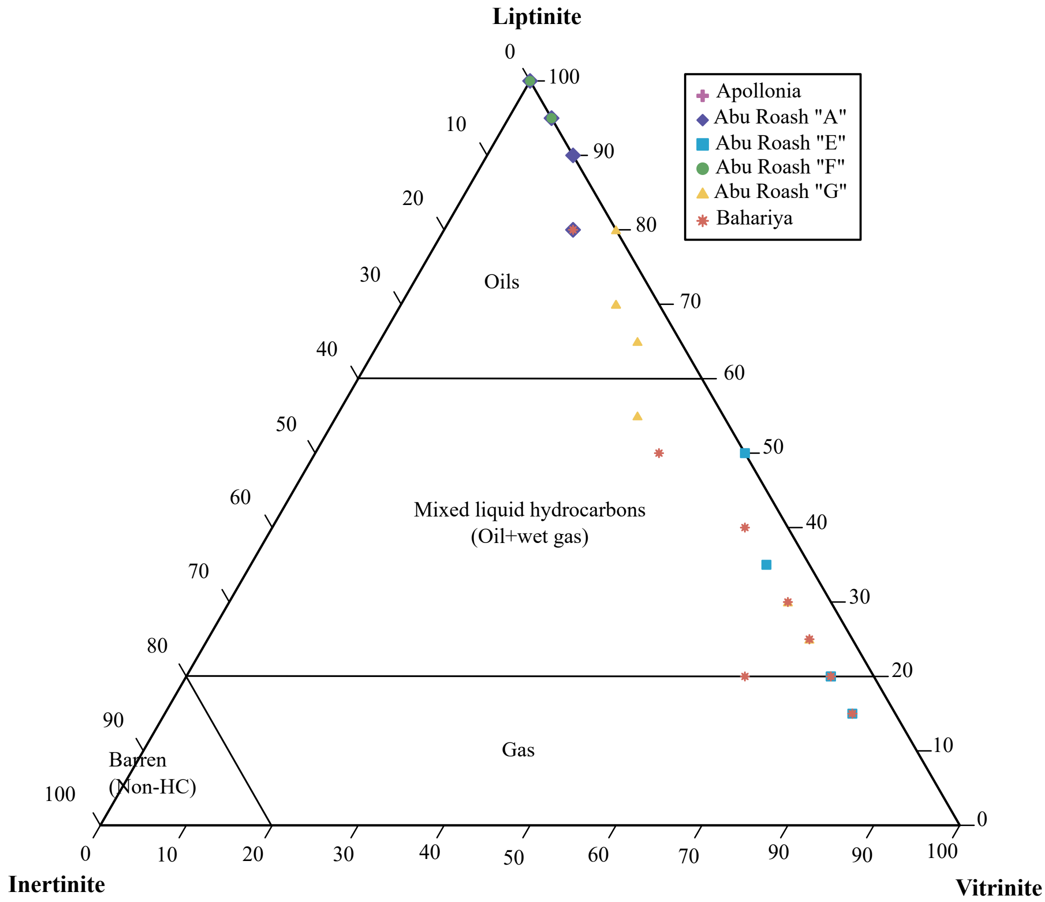
Liptinite
Inertinite
Vitrinite
Apollonia
Abu Roash "A"
Abu Roash "E"
Abu Roash "F"
Abu Roash "G"
Bahariya
Oils
Mixed liquid hydrocarbons
(Oil+wet gas)
Gas
Barren
(Non-HC)

Fig. 7

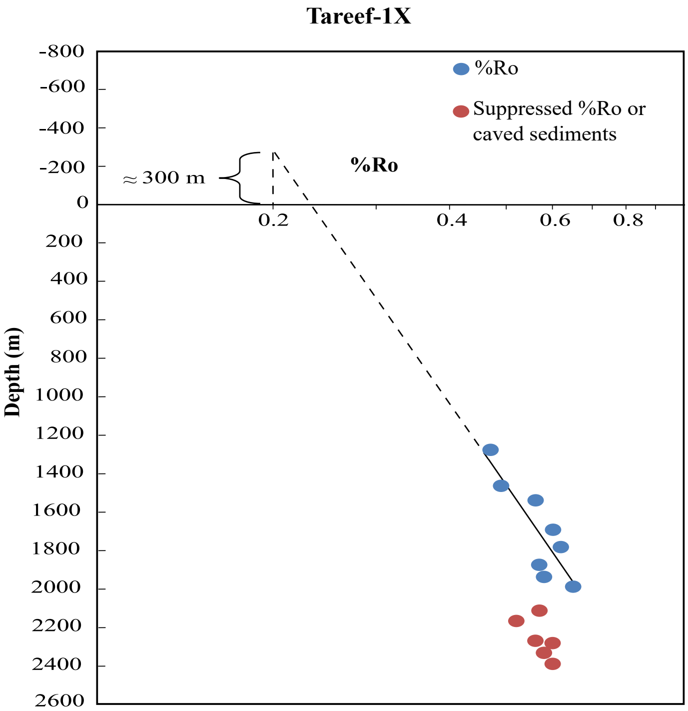

Tareef-1X
%Ro
Suppressed %Ro or caved sediments
%Ro
≈ 300 m
Depth (m)
-800
-600
-400
-200
0
200
400
600
800
1000
1200
1400
1600
1800
2000
2200
2400
2600
0.2
0.4
0.6
0.8

Fig. 8

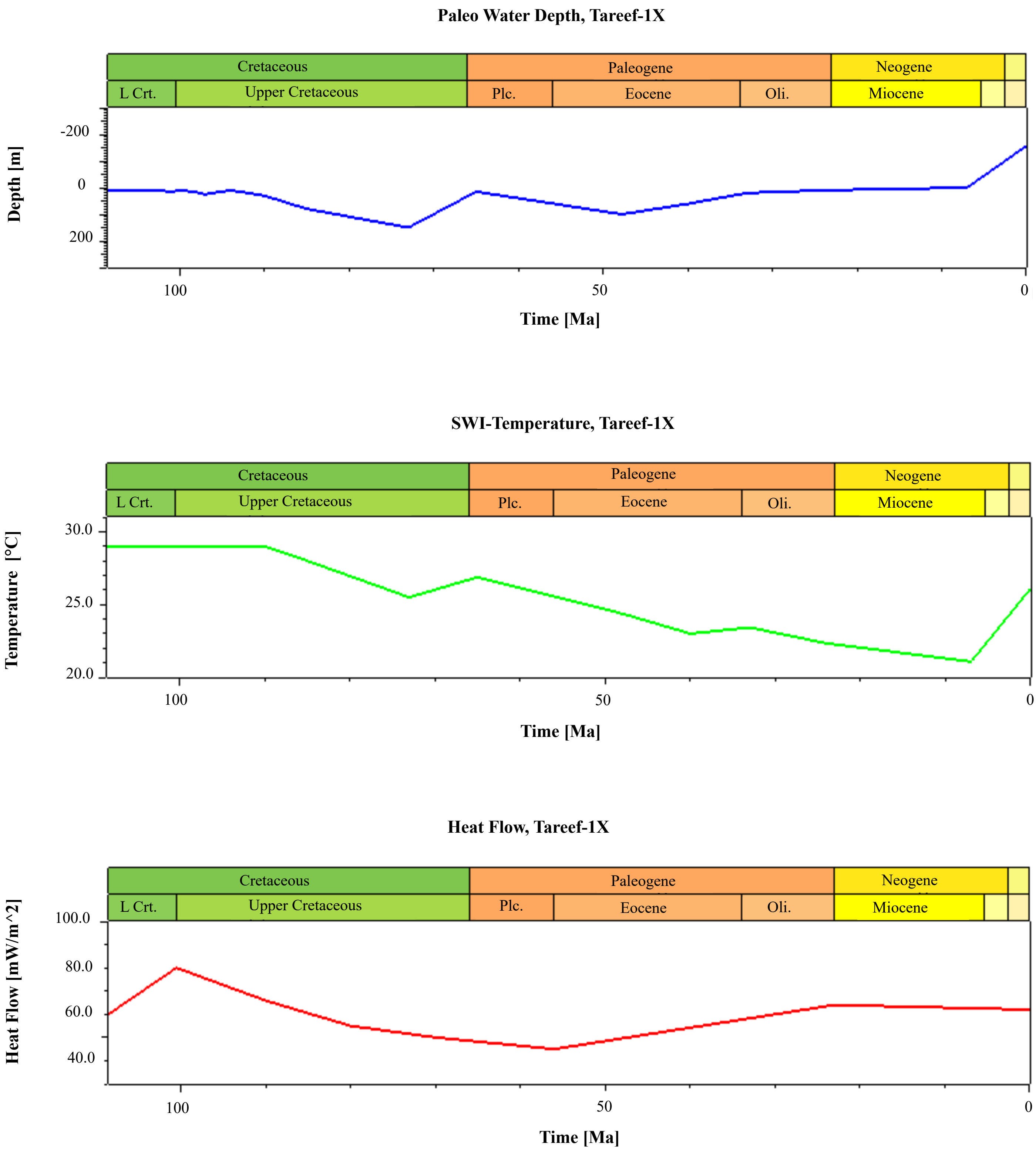
Paleo Water Depth, Tareef-1X
Cretaceous
Paleogene
Neogene
L Crt.
Upper Cretaceous
Plc.
Eocene
Oli.
Miocene
Depth [m]
-200
0
200
100
50
0
Time [Ma]
SWI-Temperature, Tareef-1X
Cretaceous
Paleogene
Neogene
L Crt.
Upper Cretaceous
Plc.
Eocene
Oli.
Miocene
Temperature [°C]
30.0
25.0
20.0
100
50
0
Time [Ma]
Heat Flow, Tareef-1X
Cretaceous
Paleogene
Neogene
L Crt.
Upper Cretaceous
Plc.
Eocene
Oli.
Miocene
Heat Flow [mW/m^2]
100.0
80.0
60.0
40.0
100
50
0
Time [Ma]

Fig. 9

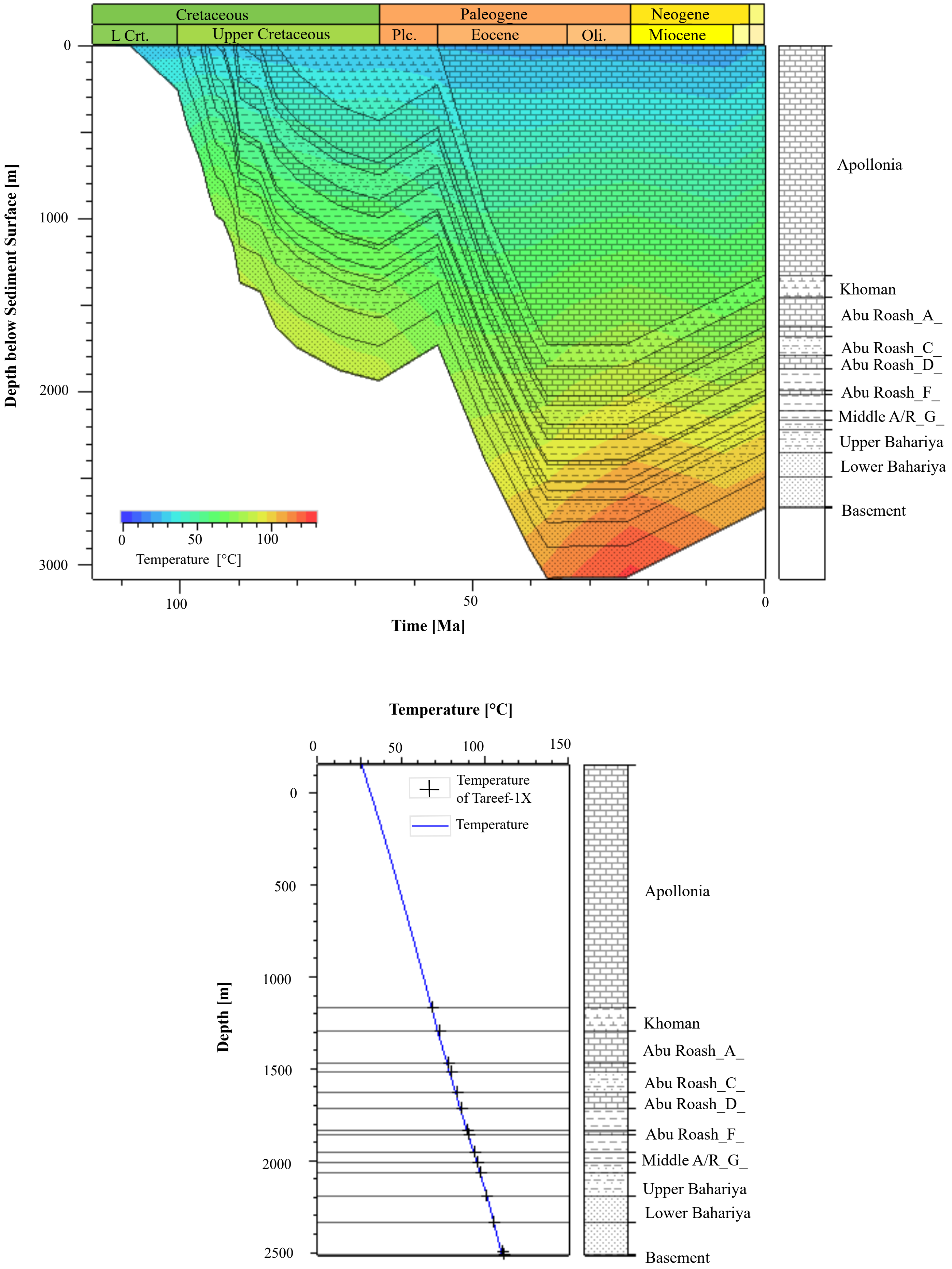

Cretaceous
Paleogene
Neogene
L Crt.
Upper Cretaceous
Plc.
Eocene
Oli.
Miocene
Depth below Sediment Surface [m]
0
1000
2000
3000
100
50
0
Time [Ma]
Temperature [°C]
Apollonia
Khoman
Abu Roash_A_
Abu Roash_C_
Abu Roash_D_
Abu Roash_F_
Middle A/R_G_
Upper Bahariya
Lower Bahariya
Basement
Temperature [°C]
0
50
100
150
Depth [m]
500
1500
2500
Temperature of Tareef-1X
Temperature

Fig. 10

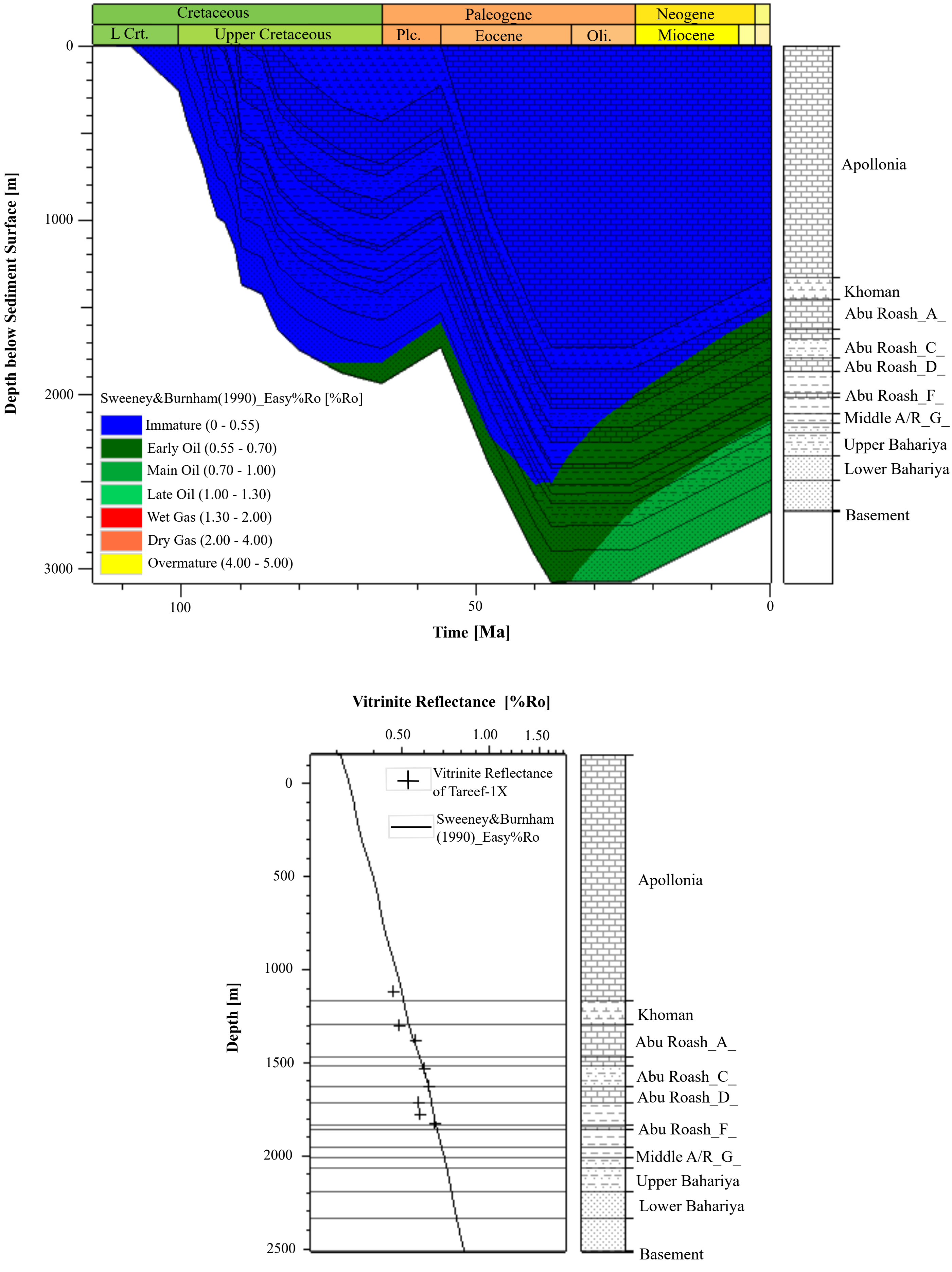

Cretaceous
Paleogene
Neogene
L Crt.
Upper Cretaceous
Plc.
Eocene
Oli.
Miocene
Depth below Sediment Surface [m]
Time [Ma]
Sweeney&Burnham(1990)_Easy%Ro [%Ro]
Immature (0 - 0.55)
Early Oil (0.55 - 0.70)
Main Oil (0.70 - 1.00)
Late Oil (1.00 - 1.30)
Wet Gas (1.30 - 2.00)
Dry Gas (2.00 - 4.00)
Overmature (4.00 - 5.00)
Apollonia
Khoman
Abu Roash_A_
Abu Roash_C_
Abu Roash_D_
Abu Roash_F_
Middle A/R_G_
Upper Bahariya
Lower Bahariya
Basement
Vitrinite Reflectance [%Ro]
Vitrinite Reflectance of Tareef-1X
Sweeney&Burnham (1990)_Easy%Ro
Depth [m]

Fig. 11

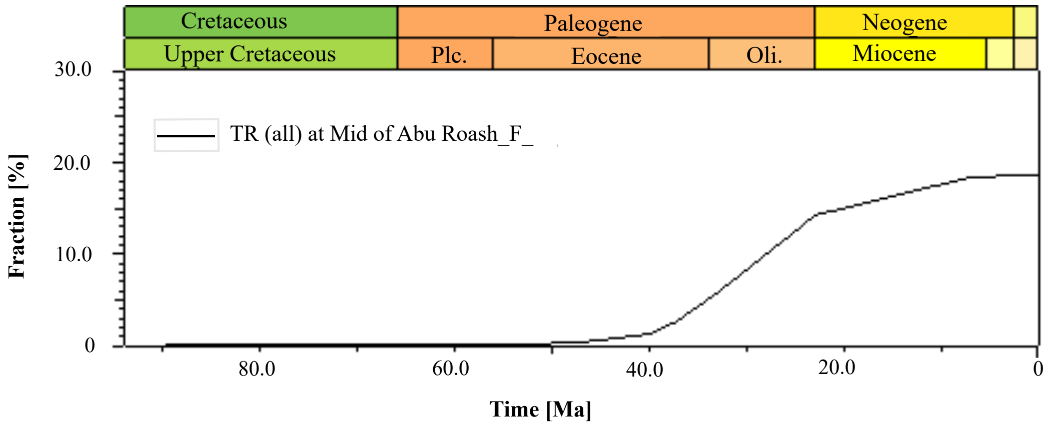
Cretaceous
Paleogene
Neogene
Upper Cretaceous
Plc.
Eocene
Oli.
Miocene
30.0
20.0
10.0
0
Fraction [%]
TR (all) at Mid of Abu Roash_F_
80.0
60.0
40.0
20.0
0
Time [Ma]

Fig. 12

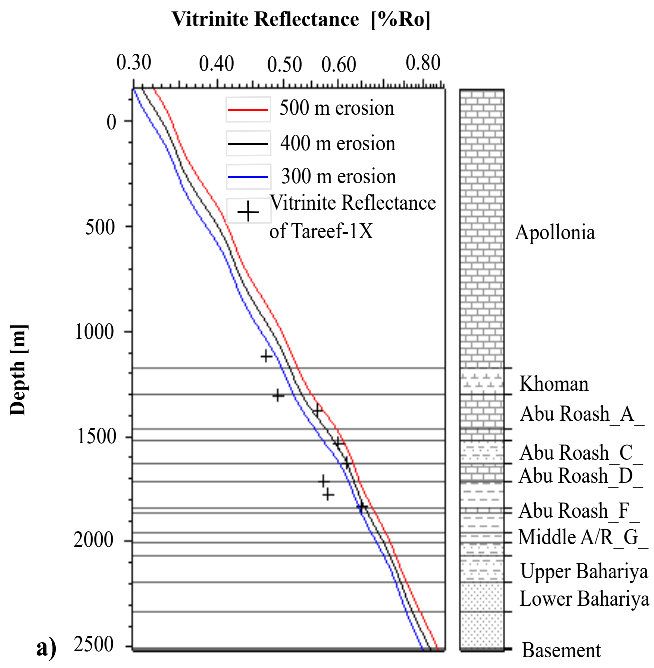

Vitrinite Reflectance [%Ro]
0.30
0.40
0.50
0.60
0.80
500 m erosion
400 m erosion
300 m erosion
Vitrinite Reflectance of Tareef-1X
Depth [m]
0
500
1000
1500
2000
2500
a)
Apollonia
Khoman
Abu Roash_A_
Abu Roash_C_
Abu Roash_D_
Abu Roash_F_
Middle A/R_G_
Upper Bahariya
Lower Bahariya
Basement

Fig. 13. a

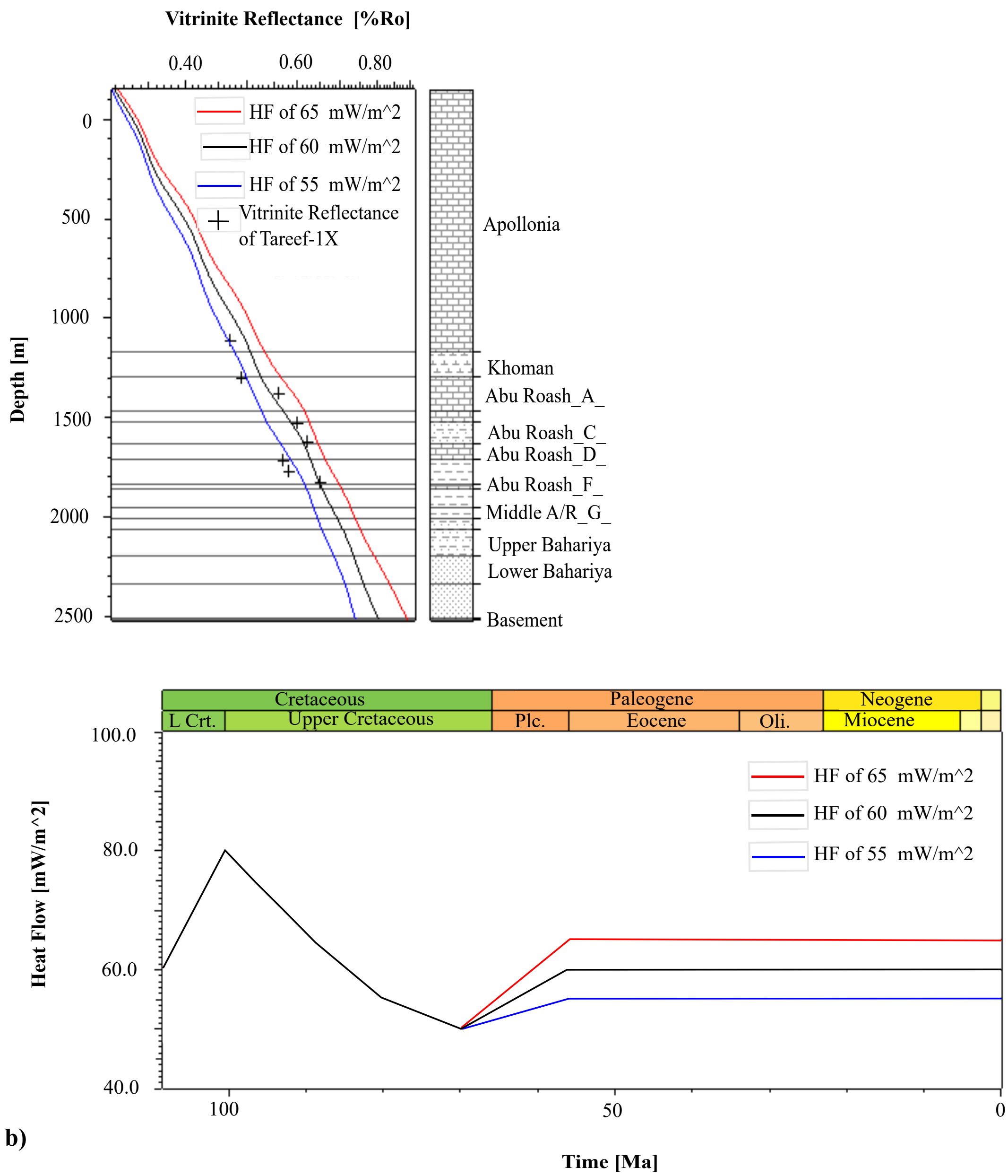
Vitrinite Reflectance [%Ro]
0.40
0.60
0.80
HF of 65 mW/m^2
HF of 60 mW/m^2
HF of 55 mW/m^2
Vitrinite Reflectance of Tareef-1X
Depth [m]
0
500
1000
1500
2000
2500
Apollonia
Khoman
Abu Roash_A_
Abu Roash_C_
Abu Roash_D_
Abu Roash_F_
Middle A/R_G_
Upper Bahariya
Lower Bahariya
Basement
Cretaceous
Paleogene
Neogene
L Crt.
Upper Cretaceous
Plc.
Eocene
Oli.
Miocene
100.0
80.0
60.0
40.0
Heat Flow [mW/m^2]
100
50
0
b)
Time [Ma]

Fig. 13. b

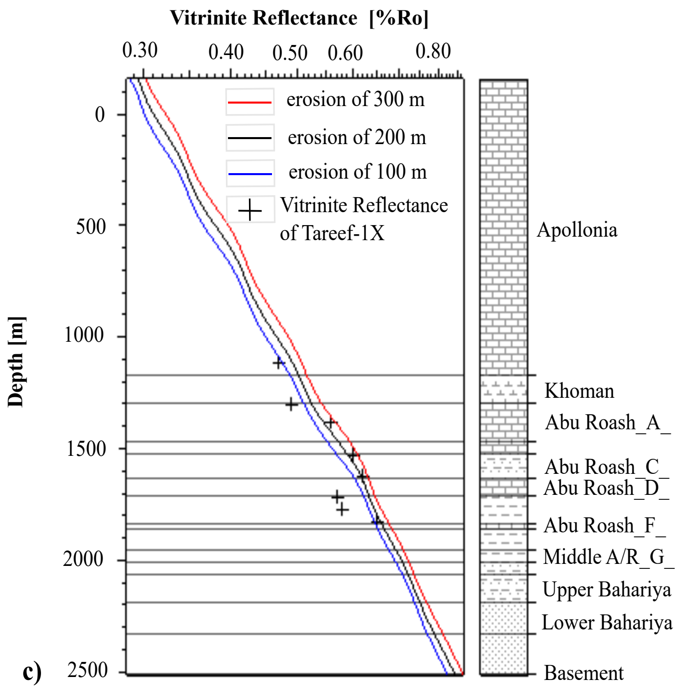
Vitrinite Reflectance [%Ro]
0.30
0.40
0.50
0.60
0.80
erosion of 300 m
erosion of 200 m
erosion of 100 m
Vitrinite Reflectance of Tareef-1X
Depth [m]
0
500
1000
1500
2000
2500
c)
Apollonia
Khoman
Abu Roash_A_
Abu Roash_C_
Abu Roash_D_
Abu Roash_F_
Middle A/R_G_
Upper Bahariya
Lower Bahariya
Basement

Fig. 13. c

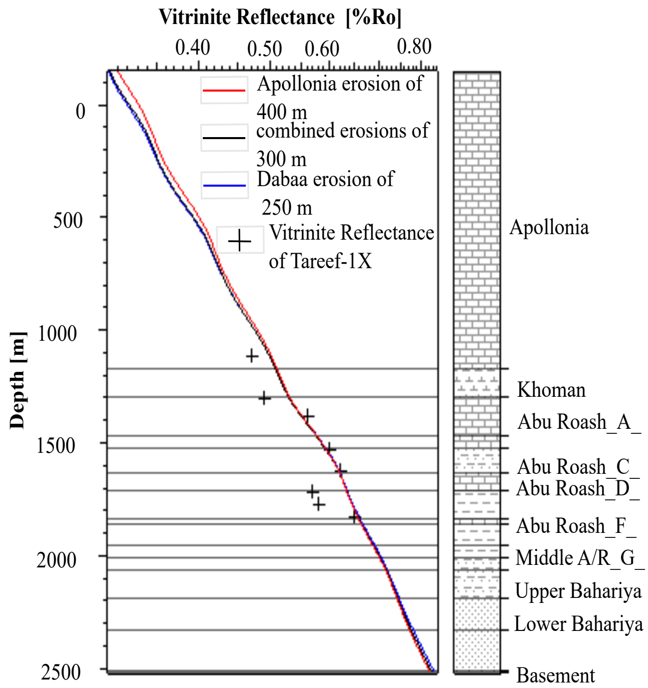
Vitrinite Reflectance [%Ro]
0.40
0.50
0.60
0.80
Apollonia erosion of 400 m
combined erosions of 300 m
Dabaa erosion of 250 m
Vitrinite Reflectance of Tareef-1X
Depth [m]
0
500
1000
1500
2000
2500
Apollonia
Khoman
Abu Roash_A_
Abu Roash_C_
Abu Roash_D_
Abu Roash_F_
Middle A/R_G_
Upper Bahariya
Lower Bahariya
Basement

Fig. 14

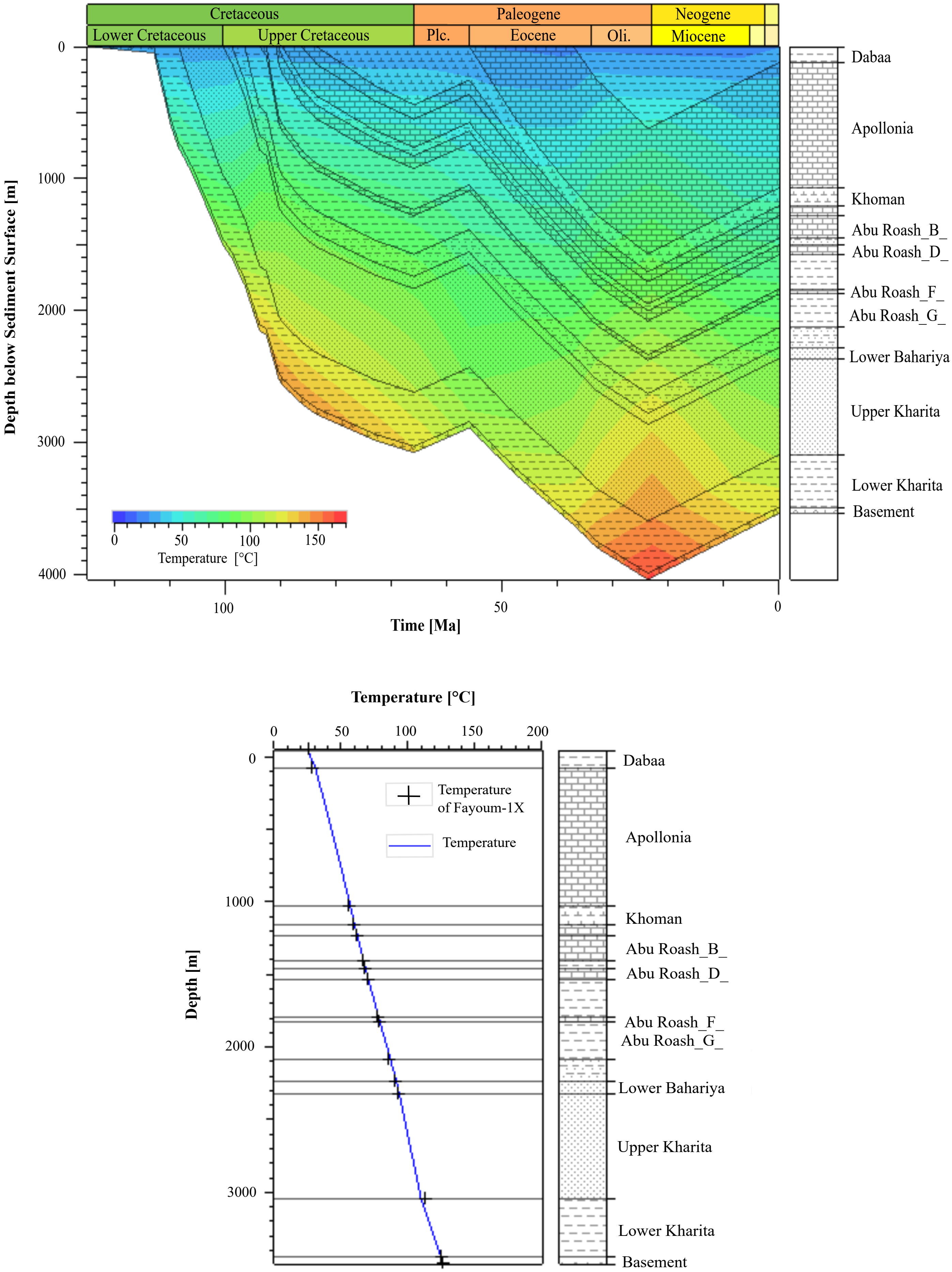

Cretaceous
Paleogene
Neogene
Lower Cretaceous
Upper Cretaceous
Plc.
Eocene
Oli.
Miocene
Depth below Sediment Surface [m]
0
1000
2000
3000
4000
Time [Ma]
100
50
0
Temperature [°C]
0
50
100
150
Dabaa
Apollonia
Khoman
Abu Roash_B_
Abu Roash_D_
Abu Roash_F_
Abu Roash_G_
Lower Bahariya
Upper Kharita
Lower Kharita
Basement
Temperature [°C]
0
50
100
150
200
Depth [m]
0
1000
2000
3000
Temperature of Fayoum-1X
Temperature
Dabaa
Apollonia
Khoman
Abu Roash_B_
Abu Roash_D_
Abu Roash_F_
Abu Roash_G_
Lower Bahariya
Upper Kharita
Lower Kharita
Basement

Fig. 15

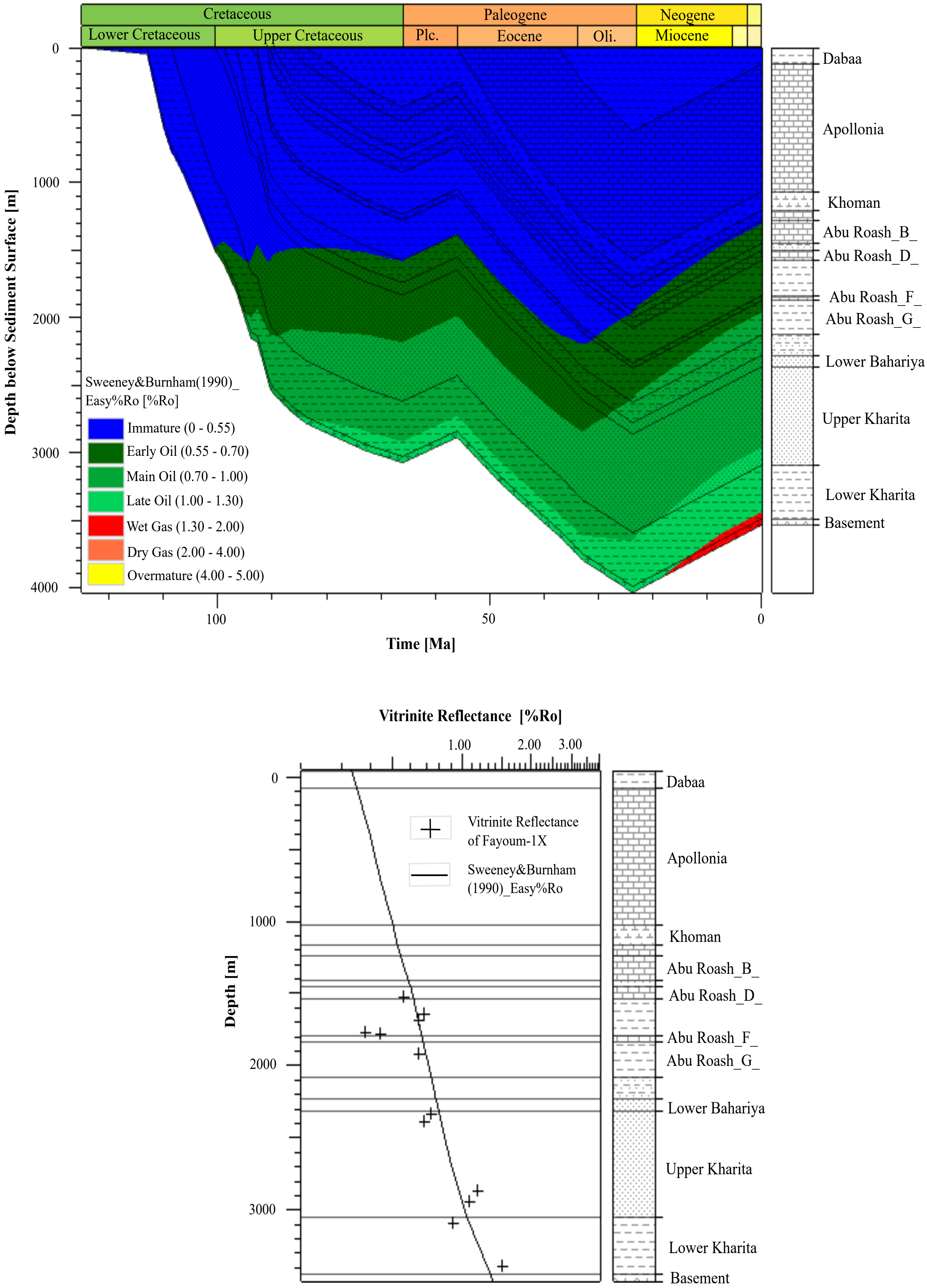
Cretaceous
Paleogene
Neogene
Lower Cretaceous
Upper Cretaceous
Plc.
Eocene
Oli.
Miocene
Depth below Sediment Surface [m]
0
1000
2000
3000
4000
Sweeney&Burnham(1990)_
Easy%Ro [%Ro]
Immature (0 - 0.55)
Early Oil (0.55 - 0.70)
Main Oil (0.70 - 1.00)
Late Oil (1.00 - 1.30)
Wet Gas (1.30 - 2.00)
Dry Gas (2.00 - 4.00)
Overmature (4.00 - 5.00)
100
50
0
Time [Ma]
Dabaa
Apollonia
Khoman
Abu Roash_B_
Abu Roash_D_
Abu Roash_F_
Abu Roash_G_
Lower Bahariya
Upper Kharita
Lower Kharita
Basement
Vitrinite Reflectance [%Ro]
1.00
2.00
3.00
Depth [m]
0
1000
2000
3000
Vitrinite Reflectance of Fayoum-1X
Sweeney&Burnham (1990)_Easy%Ro
Dabaa
Apollonia
Khoman
Abu Roash_B_
Abu Roash_D_
Abu Roash_F_
Abu Roash_G_
Lower Bahariya
Upper Kharita
Lower Kharita
Basement

Fig. 16

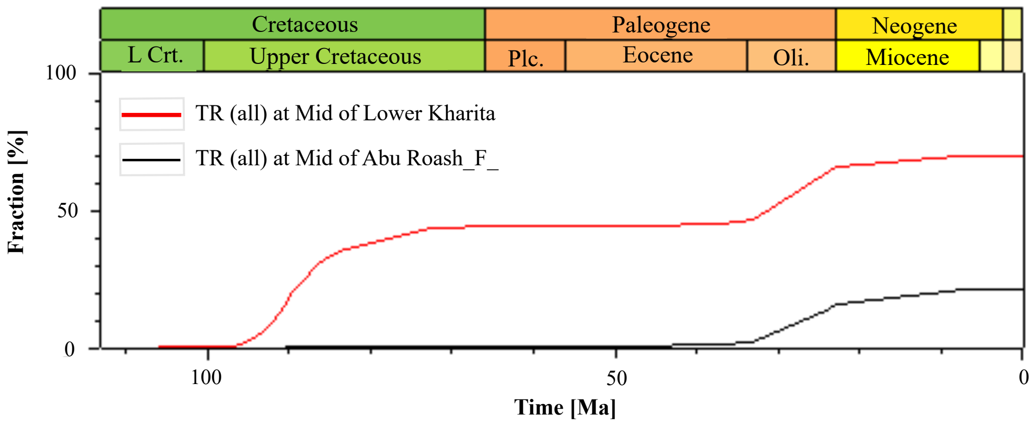
Cretaceous
Paleogene
Neogene
L Crt.
Upper Cretaceous
Plc.
Eocene
Oli.
Miocene
TR (all) at Mid of Lower Kharita
TR (all) at Mid of Abu Roash_F_
Fraction [%]
100
50
0
100
50
0
Time [Ma]

Fig. 17

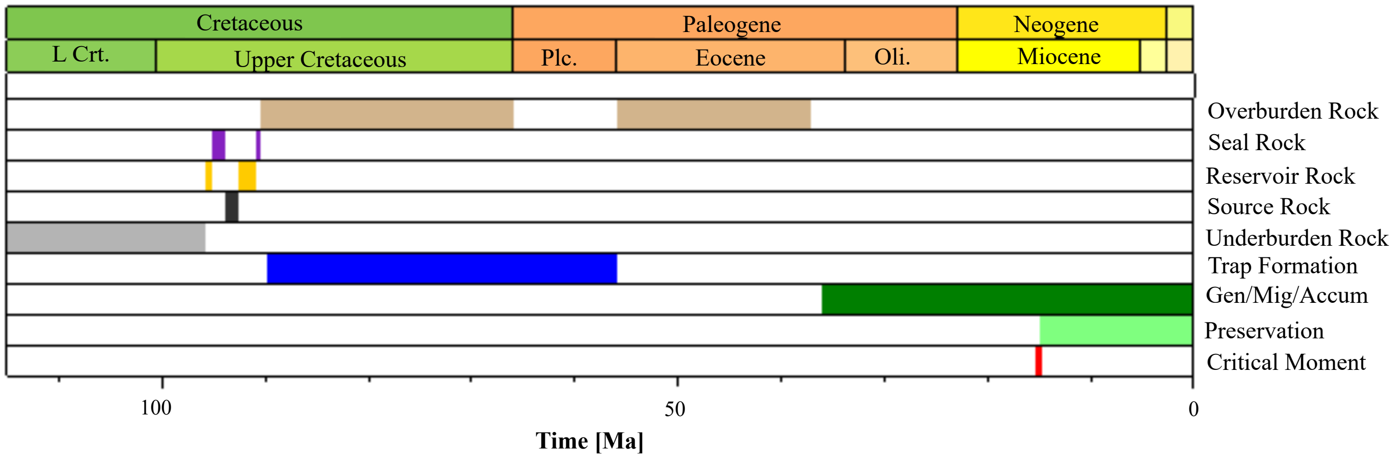
Cretaceous
Paleogene
Neogene
L Crt.
Upper Cretaceous
Plc.
Eocene
Oli.
Miocene
Overburden Rock
Seal Rock
Reservoir Rock
Source Rock
Underburden Rock
Trap Formation
Gen/Mig/Accum
Preservation
Critical Moment
100
50
0
Time [Ma]

Fig. 18

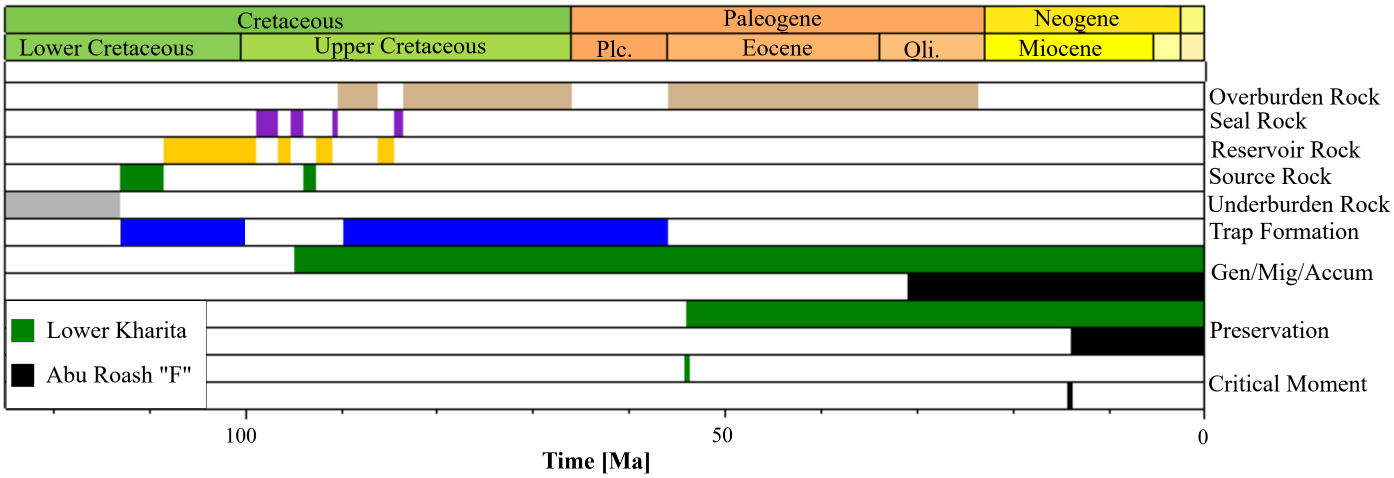
Cretaceous
Paleogene
Neogene
Lower Cretaceous
Upper Cretaceous
Plc.
Eocene
Oli.
Miocene
Overburden Rock
Seal Rock
Reservoir Rock
Source Rock
Underburden Rock
Trap Formation
Gen/Mig/Accum
Lower Kharita
Abu Roash "F"
Preservation
Critical Moment
100
50
0
Time [Ma]

Fig. 19